AD-A065 582 IIT RESEARCH INST CHICAGO ILL F/G 21/9.2
INITIATION MECHANISMS OF SOLID ROCKET PROPELLANT DETONATION.(U)
DEC 78 A N TAKATA F44620-75-C-0059
UNCLASSIFIED IITRI-J6352-3 AFOSR-TR-79-0198 NL

1 OF 1
AD
A065582

END
DATE
FILMED
5-79
DDC

UNCLASSIFIED

SECURITY CLASSIFICATION OF THIS PAGE (When Data Entered)

REPORT DOCUMENTATION PAGE		READ INSTRUCTIONS BEFORE COMPLETING FORM
1. REPORT NUMBER AFOSR-TR- 79-0198	2. GOVT ACCESSION NO.	3. RECIPIENT'S CATALOG NUMBER
4. TITLE (and Subtitle) INITIATION MECHANISMS OF SOLID ROCKET PROPELLANT DETONATION		5. TYPE OF REPORT & PERIOD COVERED Interim rept. no. 3, Nov 77 - Oct 78
		6. PERFORMING ORG. REPORT NUMBER IITRI-J6352-3
7. AUTHOR(s) A. N. Takata		8. CONTRACT OR GRANT NUMBER(s) F44620-75-C-0059
9. PERFORMING ORGANIZATION NAME AND ADDRESS IIT Research Institute, 10 West 35th Street, Chicago, Illinois 60616		10. PROGRAM ELEMENT, PROJECT, TASK AREA & WORK UNIT NUMBERS 2308A1, 61102F
11. CONTROLLING OFFICE NAME AND ADDRESS AIR FORCE OFFICE OF SCIENTIFIC RESEARCH/NA, BLDG 410, BOLLING AIR FORCE BASE, D C 20332		12. REPORT DATE December 1978
		13. NUMBER OF PAGES 54 (62 p.)
14. MONITORING AGENCY NAME & ADDRESS(if different from Controlling Office)		15. SECURITY CLASS. (of this report) Unclassified
		15a. DECLASSIFICATION/DOWNGRADING SCHEDULE

16. DISTRIBUTION STATEMENT (of this Report)

Approved for public release; distribution unlimited.

17. DISTRIBUTION STATEMENT (of the abstract entered in Block 20, if different from Report)

18. SUPPLEMENTARY NOTES

19. KEY WORDS (Continue on reverse side if necessary and identify by block number)

deflagration to detonation (DDT)
rocket motor detonation
numerical methods
propellants

20. ABSTRACT (Continue on reverse side if necessary and identify by block number)

The purpose of this study is to identify mechanisms responsible for several accidental detonations of high-energy solid rocket propellant motors. Simple models were used to predict transient gas pressures within burning propellant cracks following arrival of a stress wave. Stress waves are considered to be initiated by the propagation of a crack into a cavity containing gas at much higher pressure than that initially within the crack. Two factors were found important in creating gas pressures of similar magnitude and duration as needed to initiate propellants by impact. Namely, the generation of melt or

next page

DD FORM 1 JAN 73 1473 EDITION OF 1 NOV 65 IS OBSOLETE

UNCLASSIFIED

SECURITY CLASSIFICATION OF THIS PAGE (When Data Entered)

175 350

12

Engineering Research Division
IIT Research Institute
10 West 35th Street
Chicago, Illinois 60616

Third Interim Report

Contract F44620-75-C-0059
IITRI Project J6352

INITIATION MECHANISMS OF SOLID ROCKET PROPELLANT DETONATION

Prepared by
A. N. Takata

for

Air Force Office of Scientific Research
Bolling AFB, DC 20332

December 1978

FOREWORD

The objective of this project is the understanding of the mechanisms controlling the transition from deflagration to detonation in solid propellant rocket motors. This interim report covers the period from November 1977 through October 1978. The study was sponsored by the Air Force Office of Scientific Research (AFOSR), Directorate of Aerospace Sciences, United States Air Force under Contract F44620-75-C-0059. The program was monitored by Dr. J. S. Masi and Captain R. F. Sperlein of AFOSR.

IIT Research Institute personnel who contributed to this research are H. S. Napadensky, A. N. Takata and A. H. Wiedermann.

Respectfully submitted,
IIT RESEARCH INSTITUTE

A. N. Takata
Senior Research Engineer

APPROVED:

H. S. Napadensky
Engineering Advisor
Manager, Fire and Safety Research

CONTENTS

LIST OF ILLUSTRATIONS

LIST OF TABLES

1. INTRODUCTION

In recent years high-energy propellants have been developed containing cyclotetramethylenetranitramine (HMX) to improve the performance of rocket motors. In developing such propellants, several accidental explosions have occurred during rocket motor firings. The objective of this study is to identify the causes of the explosions so that such occurrences may be prevented in the future.

Of prime concern is the identification of factors causing pronounced pressure transients within cracks, flaws, or debonds that may produce detonation. During this and previous IIT Research Institute (IITRI) studies [1], [2], [3],* a wide variety of exploratory analyses were conducted. Their purpose was to:

- identify mechanisms and propellant properties causing pronounced pressure transients within burning cracks,
- compare predicted pressure transients with shock wave pressures/durations known to initiate propellants, and
- design experiments with which to complement the analytical study and validate its predictions.

Initial studies [1] considered the propagation of a crack into a region of high-pressure high-temperature gas such as a motor cavity. This problem is illustrated in Figure 1A. The result of sudden exposure of a crack to high-pressure high-temperature combustion gases yields:

1) Rapid ignition of the propellant surfaces and minimal times for crack expansion
2) Stress waves that act to partially collapse cracks (say after reflection from the motor case).

This study indicated that stress waves produce accelerating burn rates that lead to pronounced pressures. Burning rates and pressures vary considerably with crack location. Crack expansion produced by elevated pressures act to moderate pressure rises.

---
* Bracketed numbers refer to references listed at the end of report.

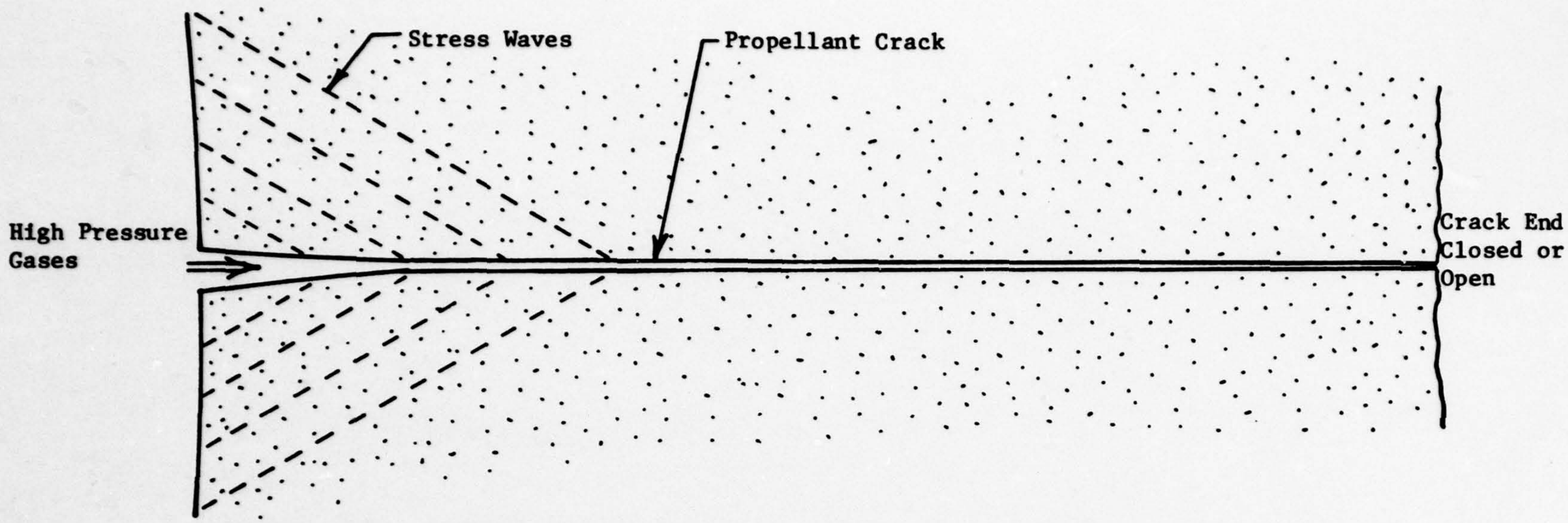

Figure 1A. Effects of Sudden Exposure of Crack to High Pressure Cavity Gases

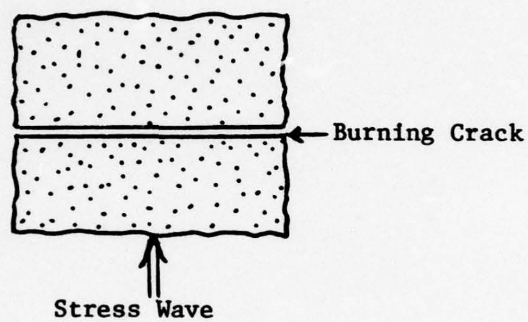

Figure 1B. Effects of Stress Waves upon Burning Cracks

Next a portion of a crack was studied as indicated by Figure 1B. It showed that the magnitude and duration of the pressure transients are highly dependent upon the amount of heat stored near the propellant surface. Once the excess heat is expended, pressures decrease as the crack continues to expand. This result points up the importance of a melt or foam layer. Without a foam the pressure transients were not sustained long enough to be a viable cause of detonation.

For this reason this past year was expended in upgrading the IITRI computer code to study the consequences of a foam layer. The revised code provides dynamic predictions of crack widths, burning rates, gas pressures, foam masses, and temperature profiles within the solid propellant of a crack element. Burning/crack conditions are considered uniform along the length of the crack element. The rate of gas loss from the crack element is constant with respect to time. It equals the rate of mass addition from the burning propellant just prior to arrival of the stress wave.

The result is a one-dimensional computer code with which to:

- identify propellant properties and crack/stress wave conditions promoting pronounced pressure transients
- assess consequences of multiple burning cracks in which pressure transients are intensified from crack to crack due to stress wave amplification.

Predicted pressure transients varied widely with propellant properties and crack conditions. Under certain crack conditions it was possible to generate pressures of the order of 10 kbars that persist for times of the order of microseconds (μsec). Such pressures are similar in magnitude and duration to those known to initiate a composite HMX material by impact 4.

In the remainder of this report the analytical basis of the computer code, and predictions and conclusions drawn from the study are presented. Included are the design of experimental means for validating computer code predictions.

2. ANALYTICAL/COMPUTATIONAL PROCEDURES

The computer code predicts pressure transients by means of the two models described:

(1) Burn model that predicts propellant burning dynamically on terms of

- temperatures within molten and solid propellant as a function of depth
- gas pressures within the crack

(2) Gas/crack model that predicts gas pressures and crack widths dynamically in terms of

- stress wave amplitude
- thermodynamic properties of the combustion gases
- propellant burning rate

In this section the analytical basis of the above computer routines are described. Nomenclature is presented following Section 4.

2.1 Burn Model

The burn model provides for various modes of propellant heating. Prior to propellant ignition, the heat flow is by convection from the gas stream. After ignition there are two sources of propellant heating. The first is by conduction from the flame; the second is by heat generated internally within the melt or foam layer. The latter is termed internal heating.

Figure 2 represents symbols used to represent various temperatures (T_f, T_m, T), heat fluxes (q_f, q_p, q) and regression rates (r_f, r) associated with the melt or foam layer and the two interfaces of the foam layer.

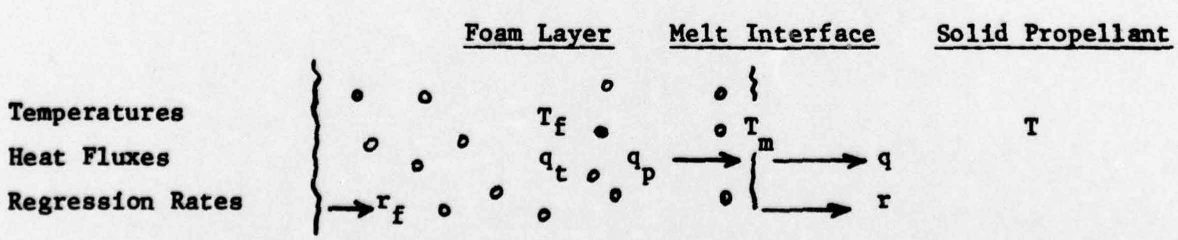

Figure 2. Principal Variables of Burn Model

2.1.1 Melt or Foam Layer

Rates of heating q_f of the foam layer during burning are described by an equation developed by Krier [5]. Introducing the heat of fusion Q_m, at the specific heats C_p and C_m of the solid and molten propellant, respectively, into his equation yields

$$q_f = \frac{\rho \bar{r}_f^2 (P)}{r_f}[C_p(T_m-T_o) + C_m(\bar{T}_f(P) - T_m) + Q_m - Q_s] + \rho_{rf}Q_s + \rho r_f(C_m - C_g)(T_f - \bar{T}_f(P)) \tag{1}$$

Here q_f represents the rate at which the foam layer is heated by heat conduction from the flame and by heat generation within the melt layer (internal heating). Bars over variables indicate values associated with steady burning at the given pressure P. Heat fluxes q_f increase as the pressure P and/or burning rate r_f rise. The two major terms of Equation (1) that induce increased heating rates are $\bar{r}_f^2(P)$ and $\rho r_f Q_s$ (internal heating). The dependence of q_f upon P and r_f changes as the burning becomes more dynamic. During near-steady burning, P and r_f are of essentially equal importance. As the burning becomes increasingly dynamic, the heating becomes more dependent upon r_f and less dependent upon P. Upward of 90 percent of the rate of the heating is attributed to internal heating during periods of highly dynamic burning.

Steady burning rates $\bar{r}_f$ are described conventionally [5] as a function of pressure P by

$$\bar{r}_f(P) = aP^n \tag{2}$$

where a and n are constants that are determined experimentally. Nonsteady burning rates r_f are predicted in terms of the foam mass M_f and foam temperature T_f using the following Arrhenius relationship

$$r_f = M_f Z \exp(-E/T_f)/\rho \tag{3}$$

In Equation (3) the expression $Z \exp(-E/T_f)$ represents the rate of gasification of the foam in a fractional basis at the temperature T_f.

Changes of the foam sensible heat Q_f are referenced to the melt temperature T_m as

$$\dot{Q}_f = q_f - q_p - \rho r_f C_m (T_f - T_m) \tag{4}$$

where q_p represents the rate of heat convection from the foam to the melt interface, and the last term represents the rate of heat loss carried away by escaping gases.

Rates of change of the foam mass M_f are described by

$$\dot{M}_f = \rho(r - r_f) \tag{5}$$

where r represents the rate of melting of the solid propellant.

Foam temperarures T_f at any time are given by

$$T_f = \frac{Q_f}{C_m M_f} + T_m \tag{6}$$

2.1.2 Melt Interface

Heat fluxes differ on either side of the melt interface. At the foam side a heat flux q_p enters the interface; at the solid-propellant side a heat flux q leaves the interface. The difference between the two fluxes is expended in melting the propellant so that

$$q_p - q = \rho r Q_m \tag{7}$$

The heat flux q_p is described in terms of a heat-transfer coeffecient h by

$$q_p = h(T_f - T_m) \tag{8}$$

Clearly h depends upon movements of the foam produced by escaping gases. For this reason h is assumed to depend upon the rate of gasification in the following fashion:

$$h = c_1 \left| \exp\left(-\frac{E}{T_f}\right) \right|^{c_2} \tag{9}$$

where c_1 and c_2 are constants which remain to be determined.

Substitution of the above expression for h into Equation (8) yields the following expression for q_p:

$$q_p = c_1 \left| \exp\left(-\frac{E}{T_f}\right) \right|^{c_2} (T_f - T_m) \tag{10}$$

At the solid propellant side of the melt interface, two conditions must be satisfied.

These are

$$q = -K \frac{\partial T}{\partial x}, \text{ and} \tag{11}$$

$$T = T_m \tag{12}$$

In view of changes of the temperature distribution within the solid propellant, it is necessary to compute q numerically. The numerical procedure is presented in Subsection 2.1.4.

2.1.3 Determination of Constants c_1 and c_2 of Heat Transfer Coefficient h

Here we shall determine the constants c_1 and c_2 of Equation (9) by use of estimated foam masses during steady burning of HMX. To this end, two equations must be solved for c_1 and c_2.

The first equation is based upon Equation (10) for steady burning as follows:

$$\bar{q}_p = c_1(\exp - E/\bar{T}_f(P))^{c_2}(\bar{T}_f - T_m) \tag{13}$$

To support steady burning, $\bar{q}_p$ must also satisfy

$$\bar{q}_p = \rho\bar{r}_f[C_p(T_m - T_o) + Q_m], \tag{14}$$

Equating the above expressions for $\bar{q}_p$ and using Equation (2) yields

$$c_1(\exp - E/\bar{T}_f(P))^{c_2}(\bar{T}_f - T_m) = \rho a P^n(C_p(T_m - T_o) + Q_m) \tag{15}$$

Equation (15) represents the first of the two equations.

The second equation is obtained from Equations (2) and (3) for steady velocities $\bar{r}_f$. It is given by

$$\rho a P^n = \bar{M}_f(P)\, Z \exp(-E/\bar{T}_f(P)) \tag{16}$$

At any given pressure P all of the parameters of Equations (15) and (16) are known except for the constants c_1 and c_2, and the foam mass $\bar{M}_f$ and temperature $\bar{T}_f$ at the given pressure. To determine the constants c_1 and c_2 it is necessary to know the melt mass $\bar{M}_f(P)$ at two pressures P. In this regard, Boggs [6] has

photographed the "frozen" HMX foam layer following extinguishment of the burning by rapid pressure relief. Bogg's photographs indicate that the steady-state foam thickness decreases as the pressure increases from 1 to 102 bars. The foam layer at 34 bars is roughly 25 μm thick; at 68 bars it appears to be about half as thick as that at 34 bars of pressure.

Assuming that the density of the "frozen foam" is half the density (1.9 g/cm^3) of solid high-density HMX propellant yields

$$\bar{M}_f(34) = 0.0024 \text{ g/cm}^2 \tag{17}$$

$$\bar{M}_f(68) = 0.0012 \text{ g/cm}^2 \tag{18}$$

Substituting each of $\bar{M}_f$, P values into Equation (16) and solving for $\bar{T}_f(P)$ with the propellant properties given in the appendix yields

$$\bar{T}_f(34) = 689.5^{o}K \tag{19}$$

$$\bar{T}_f(68) = 713.0^{o}K \tag{20}$$

Substituting the above $\bar{T}_f$, P values into Equation (15) yields two equations involving the two unknowns C_1 and C_2. Solution of the two equations yields

$$c_1 = 7.6 \cdot 10^5 \text{ cal/cm}^2\text{-sec-}^{o}K \tag{21}$$

$$c_2 = 0.338 \text{ (dimensionless)}$$

The above values for c_1 and c_2 may be used in conjunction with Equations (15) and (16) to predict the foam mass during steady burning as a function of the pressure P. Results are shown in Figure 3. Notice that the foam mass decreases rapidly with increased pressure. At a pressure of 1 bar the predicted HMX foam mass is roughly four times larger than reported values [7] for PBX 9404 and Composition B, namely 0.008 and 0.010 g/cm^2, respectively. Experimental means for checking this result are described in Section 4.

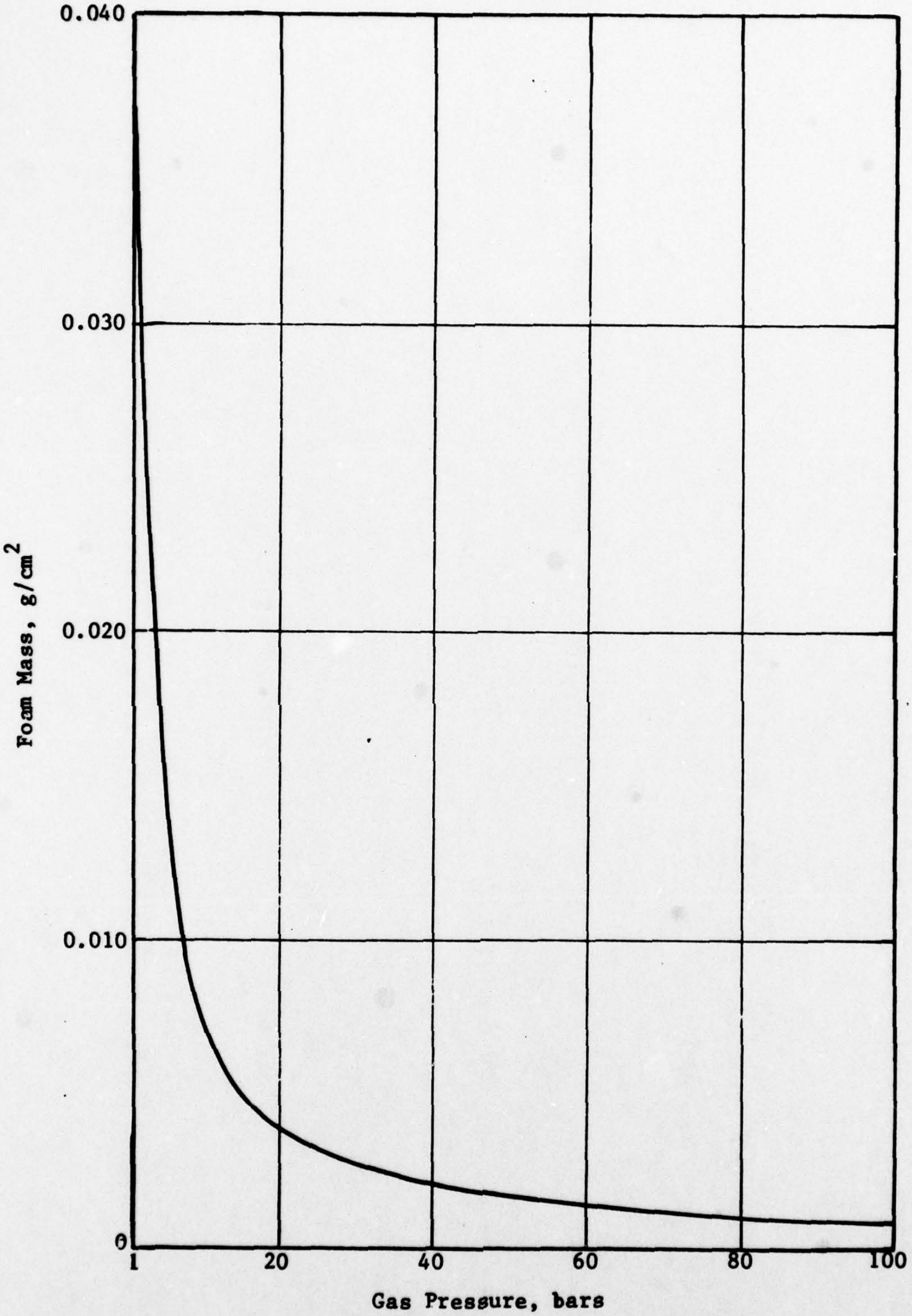

Figure 3. Predicted HMX Foam Mass as Function of Pressure during Steady Burning

2.1.4 Solid Propellant

In the burn model the depth of the propellant is assumed infinite in that heat penetrates relatively shallow depths compared to those of propellant motors. Temperatures within the solid propellant are calculated in a stepwise fashion with respect to time using a method of sources and sinks described below.

The melt interface is considered to move in a discrete fashion with respect to time within a fixed one-dimensional cartesian coordinate system as shown by the heavy lines presented in Figure 4. Prior to the start of melting, the melt interface is, of course, stationary. During each time step Δt_j following the start of melting, the melt interface moves from a depth x_{j-1} to x_j. Displacements $x_j - x_{j-1}$ of the melt interface during each time step Δt_j are represented by Δx_j.

During each time step Δt_j, a flux q'_j is applied at a specific depth x'_j between the depths x_{j-1} and x_j as shown in Figure 4. The depth x'_j is given as a fraction ζ of displacements Δx_j as

$$x'_j = x_{j-1} + \xi \Delta x_j \tag{23}$$

Selected ξ values are given in Table 1 as a function of a dimensionless parameter β and percentage changes in the rate of melting during the time step Δt_j. The parameter β is described:

$$\beta = \Delta x_j / (2\sqrt{\alpha \Delta t_j}) \tag{24}$$

The ξ values of Table 1 were precalculated and stored for the computer code. They were determined by first selecting various combinations of Δx_j and Δt_j values that satisfied Equation (24) for a given β. Each time step Δt_j and spacial increment $\Delta x'_j$ was subdivided into numerous smaller increments. Nonuniform spacial increments were used to account for exponential changes in the rate of melting. A given flux was then applied at the midpoint of each of the selected spacial increments. The increments were sufficiently small so that the exact depths at which the flux is applied is not important.

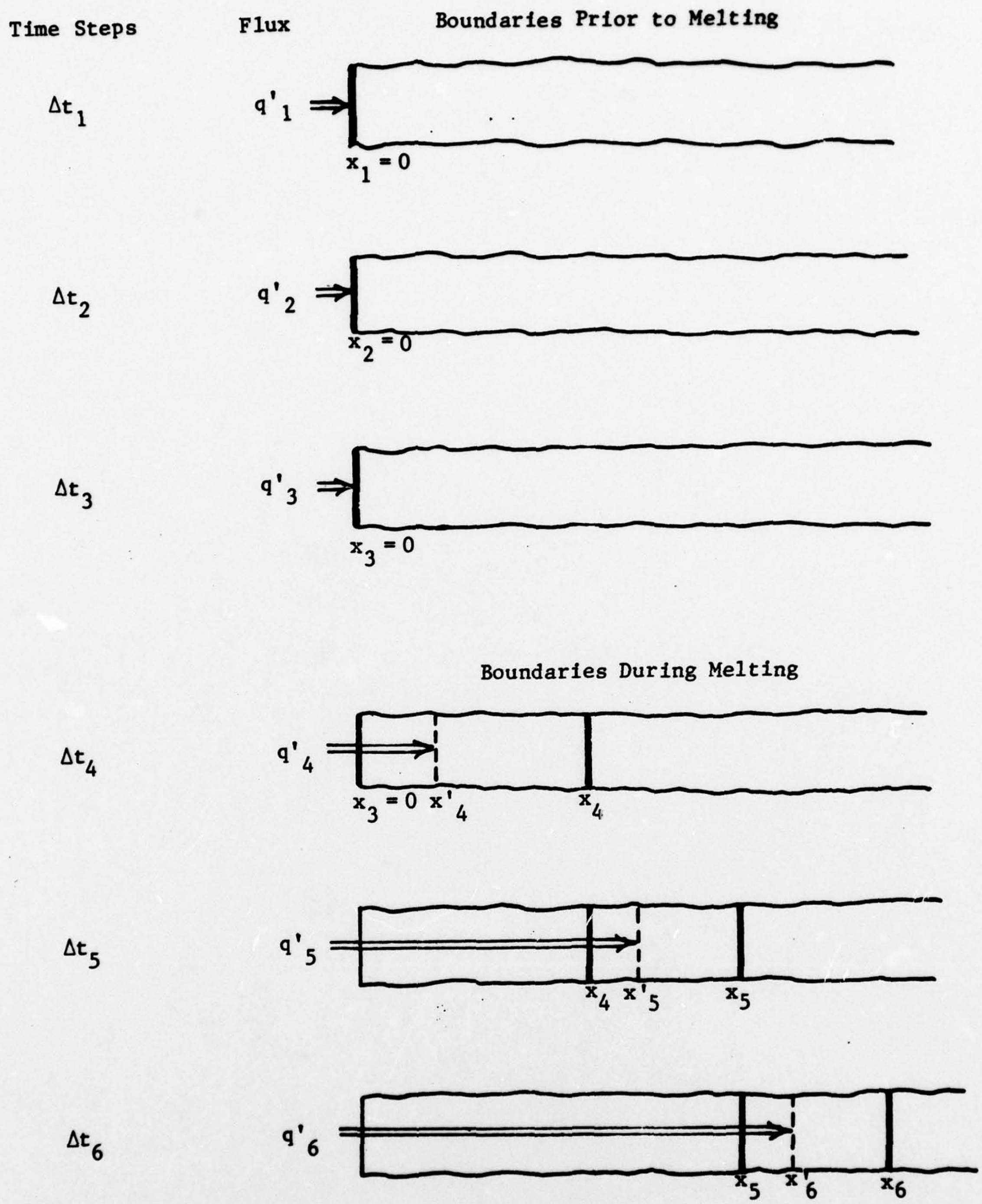

Figure 4. Application of Heat Fluxes q'_j

TABLE 1. ξ VALUES

Changes in Rate of Melting During Time Step Δt_j, percent	ξ Values (dimensionless)		
	$\beta = 0.04$	$\beta = 0.08$	$\beta = 0.12$
-80	0.289	0.295	0.300
-60	0.321	0.325	0.329
-40	0.332	0.335	0.339
-20	0.336	0.339	0.341
0	0.335	0.337	0.341
40	0.334	0.336	0.338
80	0.329	0.331	0.332
150	0.319	0.320	0.321
300	0.297	0.299	0.300
600	0.270	0.270	0.270

Then calculations were made of the total heat conducted into the propellant boundary x_j during Δt_j. Finally the depth x'_j was found at which the given flux yielded the same quantity of heat found above. Solution of Equation (23) yielded the ξ values presented in Table 1.

The consequence of introducing fluxes q'_i at various depths x'_i $(i = 1, 2, \ldots j-1)$ within the solid propellant is to create conductive fluxes at the depth x'_j. Mean conductive fluxes produced at x'_j during Δt_j by each of the prior fluxes q'_i are represented by q_{ij}. During the time step Δt_j the sum of the above fluxes is $q_{1j} + q_{2j} + \ldots q_{(j-1)j}$. Thus the mean flux q_j at x'_j during Δt_j is

$$q_j = q'_j + \sum_{i=1}^{j-1} q_{ij} \tag{25}$$

The flux q_j represents the mean flux entering the solid propellant during the given time step. It equals the q value needed to satisfy the boundary conditions given by Equations (7), (11), and (12).

The applied flux q'_j required to achieve q_j or q is found by solving Equation (25). It is given by

$$q'_j = q_j - \sum_{i=1}^{j-1} q_{i,j} \tag{26}$$

Mean conductive fluxes $q_{i,j}$ are given by

$$q_{i,j} = \frac{q'_i}{\Delta t_j} \int_o^{\Delta t_j} \left[\text{ierfc} \frac{x'_j - x'_i}{2\sqrt{\alpha(t_{j-1} - t_{i-1} + \tau}} - \text{ierfc} \frac{x'_j - x'_i}{2\sqrt{\alpha(t_{j-1} - t_i + \tau}} \right] d\tau, \quad i \leq j-1 \tag{27}$$

where $t_i = \Delta t_1 + \Delta t_2 + \Delta t_3 + \ldots . \Delta t_i$.

Prior to the start of melting $q_{i,j}$ is zero.

Temperatures within the solid propellant at the end of the time step Δt_j are given by

$$T(x) = C \sum_{i=1}^{j-1} q'_i \left[\sqrt{t_j - t_{i-1}} \ \text{ierfc} \frac{x - x'_i}{2\sqrt{\alpha(t_j - t_{i-1})}} - \sqrt{t_j - t_i} \ \text{ierfc} \frac{x - x'_i}{2\sqrt{\alpha \ (t_j - t_i)}} \right] + C\sqrt{\Delta t_j} \ q'_j$$

$$\text{ierfc} \frac{x - x'_j}{2\sqrt{\alpha \Delta t_j}} + T_o \tag{28}$$

where $C = 2/\sqrt{KPC_p}$, and the depth x equals or exceeds the depth x_i of the melt interface at the end of the time step Δt_j. At the end of the time step $T(x_j)$ equals the melt temperature T_m.

2.1.5 Validation of Computational Procedures

The computational procedure described in Subsection 2.1.4 is similar to that used in the previous report [12] to compute propellant temperatures. The only difference is the lack of a foam layer in the previous IITRI model. Computational procedures were

checked by using the previous model to calculate dynamic burn rates associated with a problem treated by Kooker [8]. Kooker performed the numerical calculations by conventional means using finite differences. Dynamic burn rates predicted by the two methods were found to be in good agreement [2].

To check the computational procedure with the presence of melting, the propellant was considered exposed to a constant heat flux starting at time zero when the propellant was unheated. The constant flux was set equal to the flux during steady burning at a selected pressure P. This problem was selected to determine whether or not appropriate steady burning conditions are achieved following a period of dynamic burning.

Steady burn velocities, foam temperatures and masses are presented in Table 2 under the columns titled "Model Predictions". Analytical predictions serve as a basis of comparison. They were obtained by solving Equations (2), (15), and (16).

It may be observed that the model predictions are in good agreement with the analytical steady-state values for each of the five pressures considered. It indicates that the cumulation of errors by the numerical calculations is relatively small.

2.2 Gas Crack Model

The gas/crack model dynamically predicts:

- pressures and temperatures of gases within the crack
- velocities of each crack wall
- crack widths

It utilizes predicted energy and mass flows into the crack from the burning propellants. The latter are supplied by the burn model.

2.2.1 Combustion Gases

Conservation of gas mass is expressed by

$$\frac{d\rho_g}{dt} = \frac{(\dot{M}_g - \rho_g \dot{C}_w)}{C_w} \tag{29}$$

while conservation of energy e is expressed by

TABLE 2. COMPARISON OF MODEL PREDICTIONS WITH STEADY-STATE ANALYTICAL PREDICTIONS

	Steady Burn Velocities, cm/sec		Foam Temperatures, ^oK		Foam Mass, g/cm^2	
Pressure, Bars	Analytical Predictions*	Model Predictions	Analytical Predictions**	Model Predictions	Analytical Predictions***	Model Predictions
1	0.030	0.030	600.8	601.3	0.03760	0.03570
10	0.217	0.216	653.2	653.9	0.00738	0.00702
32	0.591	0.599	688.5	688.7	0.00250	0.00242
50	0.867	0.861	702.5	703.3	0.00162	0.00154
100	1.574	1.560	727.1	728.1	0.00080	0.00075

* From Equation (2)
** From Equation (15)
*** From Equations (15) and (16)

$$\frac{de}{dt} = (Q_g - P\dot{C}_w - e\dot{M}_g)/(\rho_g C_w) \tag{30}$$

The mass and energy flows $\dot{M}_g$ and $\dot{Q}_g$ in Equations (29) and (30) are calculated in terms of r_f, T_f, and q_f as

$$\dot{M}_g = 2f\rho(r_f - \bar{r}_f(P_o)) \tag{31}$$

$$\dot{Q}_g = \dot{M}_g(Q_r + Q_m + C_p T_m + C_m(T_f - T_m)) - 2fq_f \tag{32}$$

The factor f represents the ratio of the area of the propellant crack surface to that of a planar surface. Reactions of the evolved gases are assumed to be instantaneous.

The term $\bar{r}_f(P_o)$ of Equation (31) is introduced to provide for a constant rate of mass loss from the element of crack. It equals the rate of mass flow into the crack element just before the stress wave arrives so that pressure uses are initiated solely by the stress wave. The effect of the mass loss upon subsequent pressure rises is relatively small due to the short times (~0.1 ms) involved in the production of the pressure transients.

Combustion gases within the crack are assumed to obey the Nobel-Abel equation of state

$$P(1/\rho_g - b) = RT_g \tag{33}$$

Internal energy e is given by

$$e = P(1/\rho_g - b)/(\gamma - 1) \tag{34}$$

where the ratio γ of the specific heats is assumed constant. In terms of e, the pressure P is given by

$$P = (\gamma - 1)e/(1/\rho_g - b) \tag{35}$$

2.2.2 Velocities of Crack Walls

The two walls of a crack move at different velocities in that only one of the crack walls is subjected to a stress wave of amplitude ΔP. The velocities of the two crack walls are represented by W_1 and W_2, where W_1 equals the velocity of the crack wall upon which the stress wave is incident.

Velocities W_1 and W_2 are considered positive when they act to increase the crack width C_w and negative otherwise. The velocity W_1 of the crack wall subjected to the stress wave is given by

$$W_1 = r_f + \frac{P + P_o - 2\Delta P}{I(P)} \tag{36}$$

The velocity W_2 of the other crack wall is

$$W_2 = r_f + \frac{P - P_o}{I(P)} \tag{37}$$

Notice that W_1 may be either positive or negative while W_2 is always positive. This, of course, is because the gas pressure and burning act to expand the crack, while the stress wave acts to contract the crack.

Rates of change of the crack width C_w are given by

$$\dot{C}_w = W_1 + W_2 \tag{38}$$

Initially a stress wave contracts a crack; thereafter elevated pressures commence to counter the effects of the stress wave so that the crack commences to expand.

2.3 Computational Procedures

Burn and gas/crack predictions are made in a stepwise fashion with respect to time. Each model uses output supplied by the other. The burn model supplied rates of energy and mass flows into the crack for the gas/crack model; the gas/crack model supplies gas pressure for the burn model. Time steps are selected by the burn model.

2.3.1 Burn Model Computational Procedures

The burn model calculates:

- foam temperatures T_f
- burn rates r_f
- melt rates r
- foam mass M_f and
- sensible heat Q_f in the foam following each time step Δt_j.

Time steps are calculated as

$$\Delta t_j = \text{minimum}\left[\frac{4\alpha\beta^2}{r_j^2}, \frac{0.1\rho r_f}{M_f}\right] \tag{39}$$

where r_j represents the mean melt velocity during Δt_j. The first expression within the brackets of Equation (39) is obtained from Equation (24). It is arrived at by replacing Δx_j by $r_j \Delta t_j$ and solving for Δt_j. The second expression is used to limit the fraction of the foam gasified during Δt_j to one-tenth.

Burn conditions are predicted by solving Equations (1) to (7), (10) to (12), and (23) to (28) by means of successive approximations. The solution is found by adjusting the melt velocity r_j until the above system of equations is satisfied.

Each trial r_j is checked by using the resultant values for the foam temperature T_f and the heat flux q_j or q into the solid propellant. The trial value is checked by substituting T_f into Equation (10) to find q_p. Then the boundary condition given by Equation (7) is solved for r. If r does not agree with the trial value r_j within 0.3 percent, r_j is revised and the calculations repeated. Usually one to three trials are needed to achieve the above accuracy.

2.3.2 Gas/Crack Model Computational Procedures

During each time step Δt_j the gas/crack model upgrades values for:

- velocities W_1, W_2 of the crack walls
- crack width C_w
- gas density ρ_g
- internal energy e
- gas temperature T_g and
- gas pressure P.

Velocities W_1 and W_2 of the crack walls are computed by substituting the burn velocity r_f and the pressure P into Equations (36) and (37). Changes of the crack width C_w are computed by

substituting the velocites W_1 and W_2 into Equation (38) and multiplying by the time step. The gas density ρ_g and the internal energy e are computed by means of Equations (29) through (32). Gas pressures and temperatures are obtained by solving Equations (33) and (35).

3. MODEL PREDICTIONS

This section is concerned with examining the influence of various factors upon pressure transients produced in burning cracks. First the consequence of altering various propellant properties and crack conditions upon pressure transients within single cracks is examined. Then the consequence of applying pressure transients (or stress waves) from one crack to the next in a sequential fashion is determined. Table 5 in the appendix describes property values used for the HMX propellant and combustion gases.

Six parameters were varied during the course of this study. Two of the six parameters are propellant properties. These are:

- internal heat Q_s
- propellant impedance I_o at ambient pressure

Remaining parameters are:

- initial crack width C_{wo}
- initial gas pressure P_o (foam temperature adjusted accordingly)
- amplitude ΔP of incident stress wave
- initial foam mass M_{fo}

The adjective "initial" refers to values immediately before the stress wave arrives. Each of the above conditions can vary widely from crack to crack depending upon how the crack develops, ignites and burns. Uncertainties also exist in the propellant properties. For these reasons, three values were chosen for each of the six parameters cited above. They are listed in Table 3.

Initial propellant temperatures were varied with the initial pressure P_o to reflect the fact that propellant heating increases with the pressure. Temperature distributions within the solid propellant are presented in Figure 20 in the appendix. Foam temperatures were set equal to their value during steady burning at the specified initial pressure P_o.

TABLE 3. PARAMETRIC VALUES SELECTED FOR SENSITIVITY STUDIES

Parameter	Nominal value ± perturbations
Q_s	150 ± 50 cal/g
I_o*	0.45 ± 0.15 bars sec/cm
C_w	0.10 ± 0.05 cm
P_o**	34 ± 17 bars
ΔP	68 ± 34 bars
M_{fo}	0.010 ± 0.005 g/cm^2

* Impedance $I = I_o$ (1+0.0002 P(bars))

** Foam temperature and temperature distribution in solid propellant varies with P_o as described by Figure 20 in the appendix.

Values of the internal heat Q_s and propellant impedance I_o were estimated. The Q_s values are slightly smaller than cited in the literature [9] for HMX. The values for the initial gas pressure P_o and the amplitude ΔP of the incident stress wave are considered typical of the magnitudes one may encounter in a crack. In this regard P_o varies with time and gas flow into a crack while ΔP depends upon the cavity pressure and rocket motor geometries.

Foam masses M_{fo} presented in Table 3 are larger than the values presented in Figure 3 for steady burning at the pressure P_o. Implicit in this assumption is relatively low heating rates prior to ignition, or the cumulation of melt due to melt flow by gas flow into the crack.

To better appreciate model predictions a few salient features of the problem should be noted. First burning will accelerate whenever the foam mass and/or temperature exceed their steady-state values at the given pressure. Foam masses may be augumented by the processes described in the previous paragraph. Foam temperatures will increase with pressure in that increased pressures raise the foam heating. Pressure increases are initiated by stress waves

acting to partially collapse cracks. Thereafter pressure increases are sustained by accelerated burning and by the stress wave acting to retard crack expansion caused by elevated gas pressures.

A key factor in the production of pronounced pressures is the amount of readily available foam present. In this regard the amount of foam needed to maintain burning decreases as the pressure rises. Transient burning continues until the "excess" foam or "melt" is expended. That is why large foam masses are conducive to detonation.

Figure 5 is presented to illustrate salient features of the problem. It presents transient crack widths, melt masses and pressures using the unperturbed values presented in Table 3. Time starts with the arrival of the given stress wave.

Initially the stress wave partially collapses the crack. The result is increased gas pressures which cause increased propellant heating (see Equation (1)). The result is accelerated burning that supports progressive increases of the pressure.

Early during the pressure buildup the crack commences to expand in response to the elevated pressures. Pressures continue to rise during crack expansion until the "excess melt" is consumed by burning. The pressure spikes are due to the fact that much of the melt is consumed within short times of the order of a few μseconds. Thereafter the burning rates and pressures commence to decrease due to continued crack expansion.

3.1 Consequences of Varying Individual Parameters

This section indicates the effect of perturbing individual parameters upon pressure transients and crack widths. The perturbations in question were presented previously in Table 3.

Figures 6 and 7 show the effect of varying the propellant properties Q_s and I_o, respectively. Figure 6 indicates that higher internal heats Q_s promote higher pressures at earlier times. The latter is due to greater propellant heating with higher Q_s values.

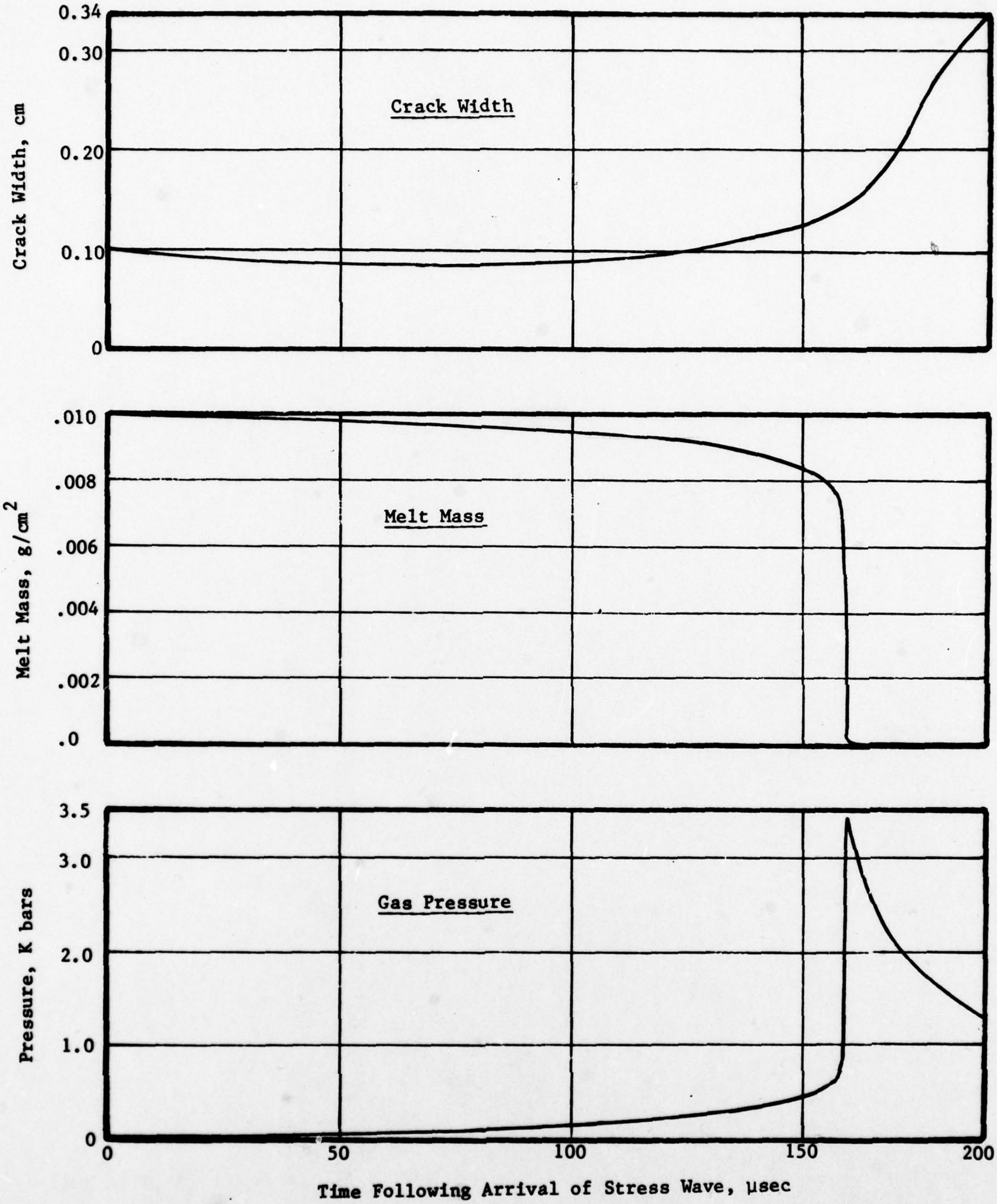

Figure 5. Transient Predictions for Case 2 Conditions

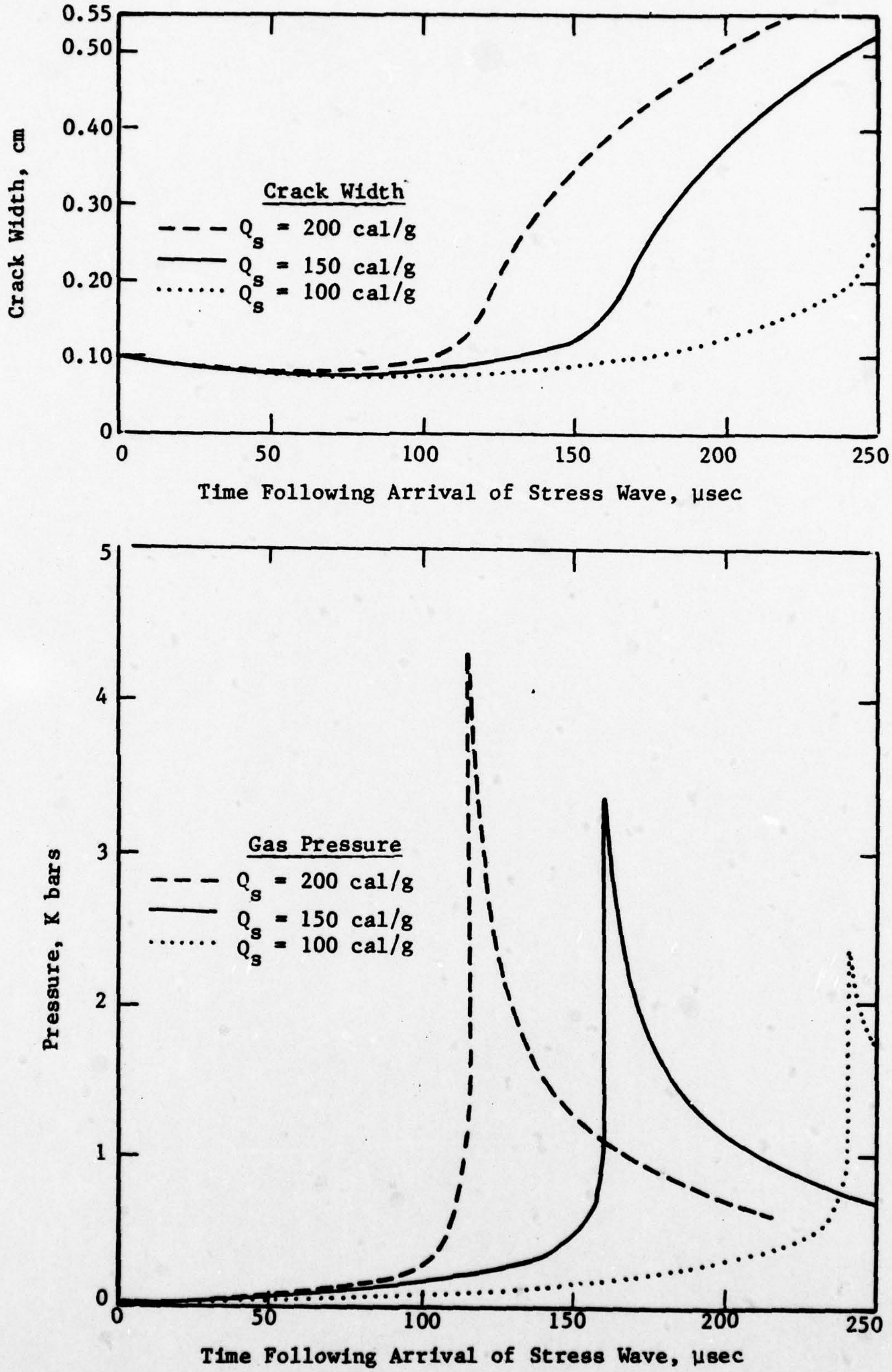

Figure 6. Consequences of Varying Internal Heat (Q_s)

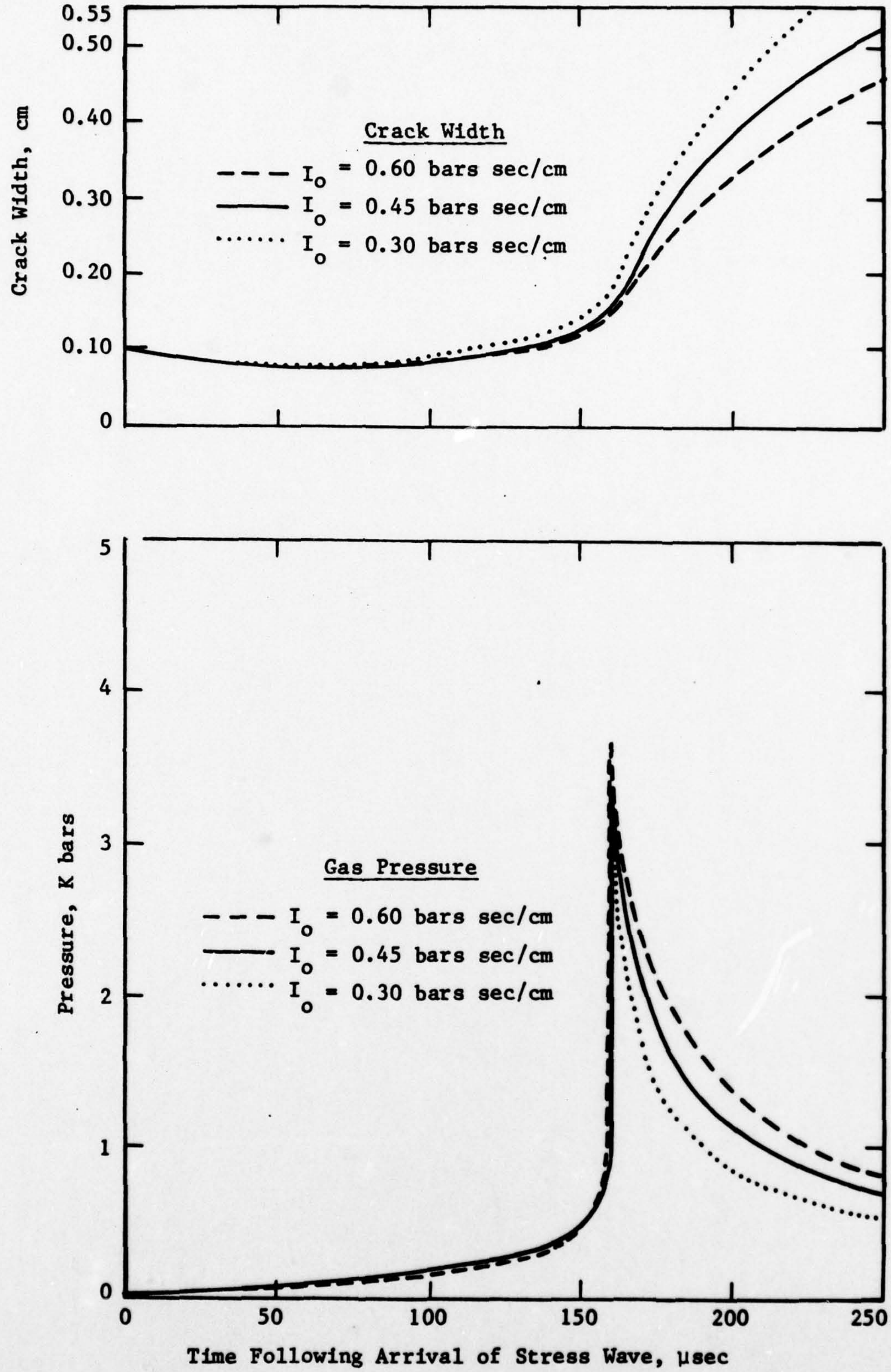

Figure 7. Consequences of Varying Propellant Impedances (I_o)

Figure 7 indicates that slightly higher pressures will occur with propellants with higher impedances I_o. The higher pressures are primarily a consequence of less crack expansion.

In Figure 8 the initial pressure P_o and foam temperature were varied simultaneously. The figure shows that the increased initial pressures and foam temperatures produce substantial pressure increases at earlier times. The pressure increases are due to more rapid consumption of the "excess melt or foam" which in turn yields smaller cracks at the time at which the pressures peak.

Figures 9 and 10 indicate consequences of varying the initial crack width C_{wo} and the amplitude ΔP of the initial stress wave. Smaller crack widths C_{wo} or higher stress wave amplitudes ΔP increase gas pressures by lowering the crack volume. For the given values, the pressure transients are not highly dependent upon the initial crack width or the amplitude of the incident stress wave.

Figure 11 shows the effect of varying the initial foam mass M_{fo}. As indiacted earlier larger foam masses produce more pronounced pressures. There are two reasons for the higher pressures. The first is the larger amounts of gas evolved. The second is the more rapid gasification of the foam layer. The latter is explained by the cooling effects of the molten propellant entering the foam. Temperatures rises are inhibited less by the incoming melt with layer foam masses. The result is more rapid gasification of the "excess foam". In turn rapid gasification yields less time for crack expansion and hence higher pressures.

3.2 Consequence of Varying All Parameters Simultaneously

In this section three sets of values for the six parameters presented in Table 3 are used to gain a better appreciation of the range of pressures that may be produced in cracks. The three sets of values are presented in Table 4.

The case 2 values represent nominal values presented in Table 3. The case 1 values represent perturbed values that yielded the smallest pressures; the case 3 values are perturbed values that yielded the highest pressures.

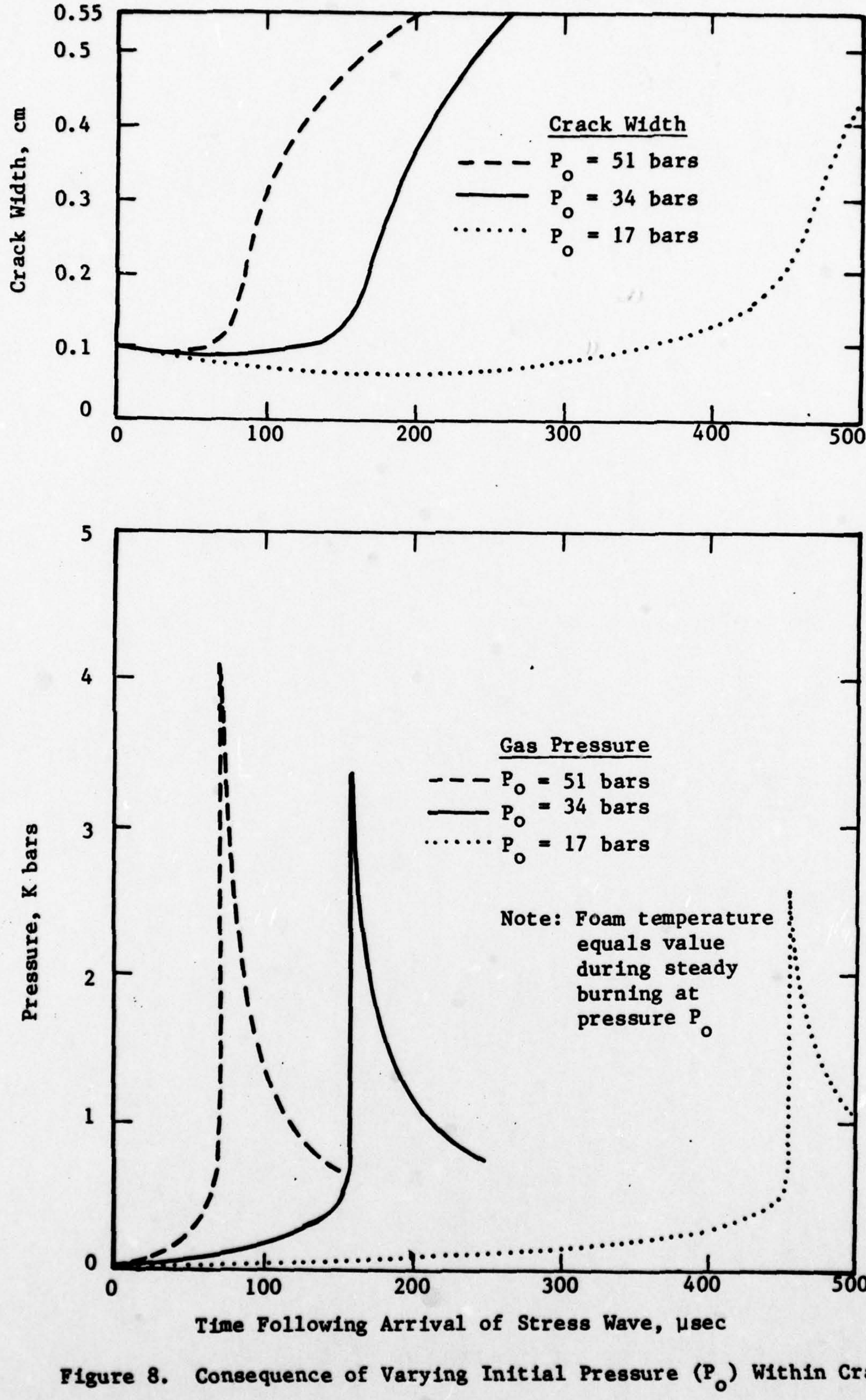

Figure 8. Consequence of Varying Initial Pressure (P_o) Within Crack

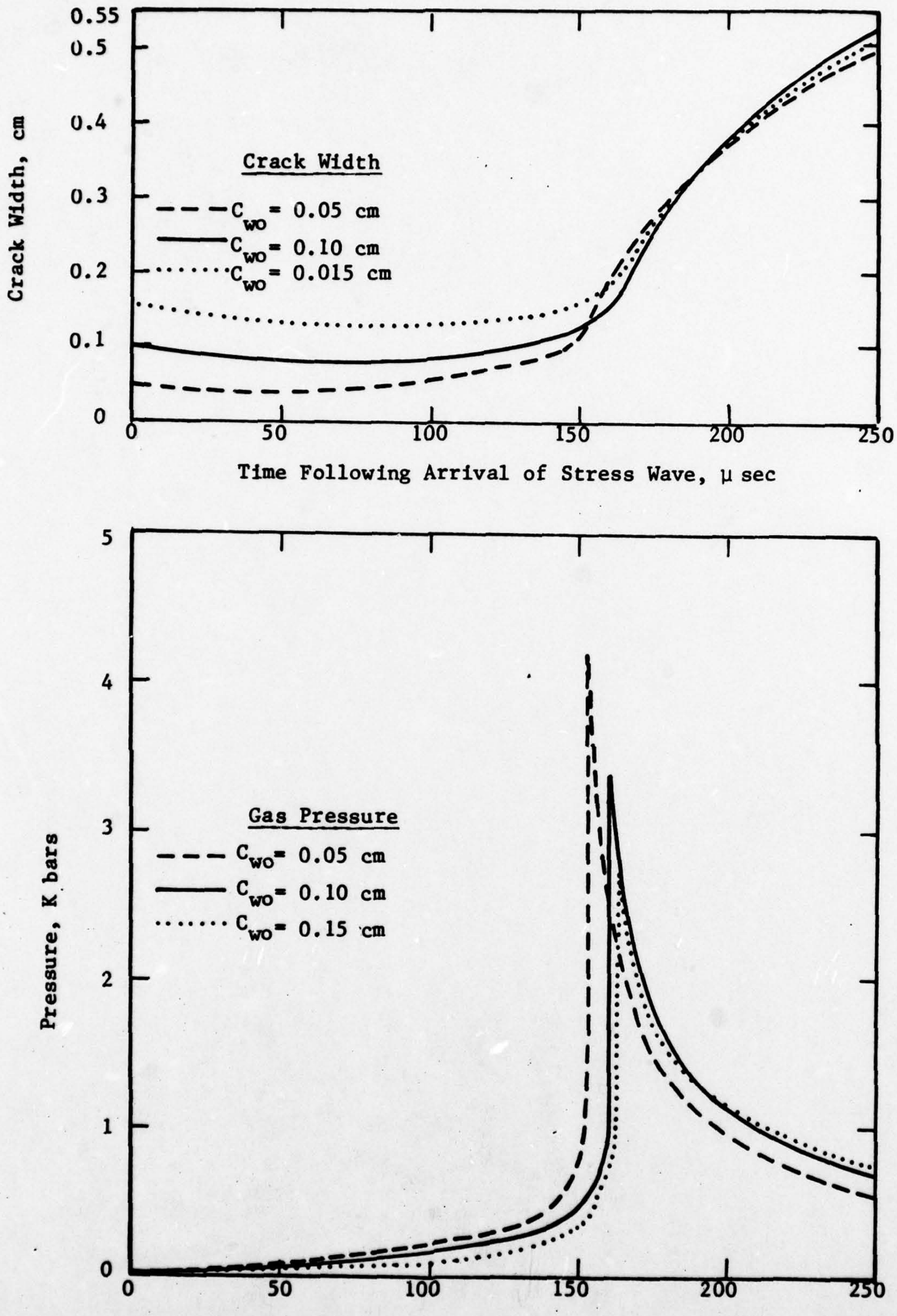

Figure 9. Consequences of Varying Initial Crack Width (C_{wo})

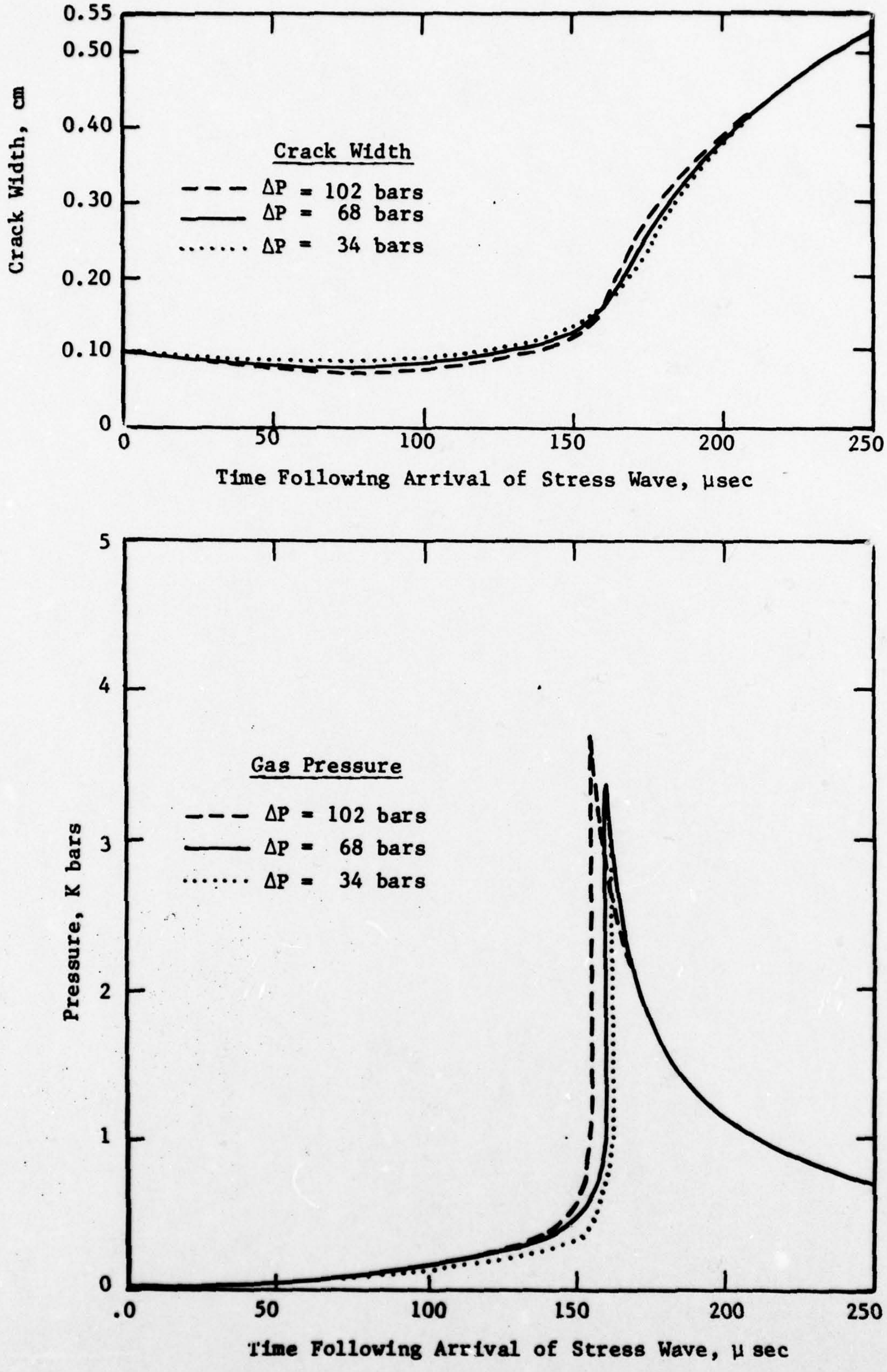

Figure 10. Consequences of Varying Amplitude (ΔP) of Incident Stress Wave

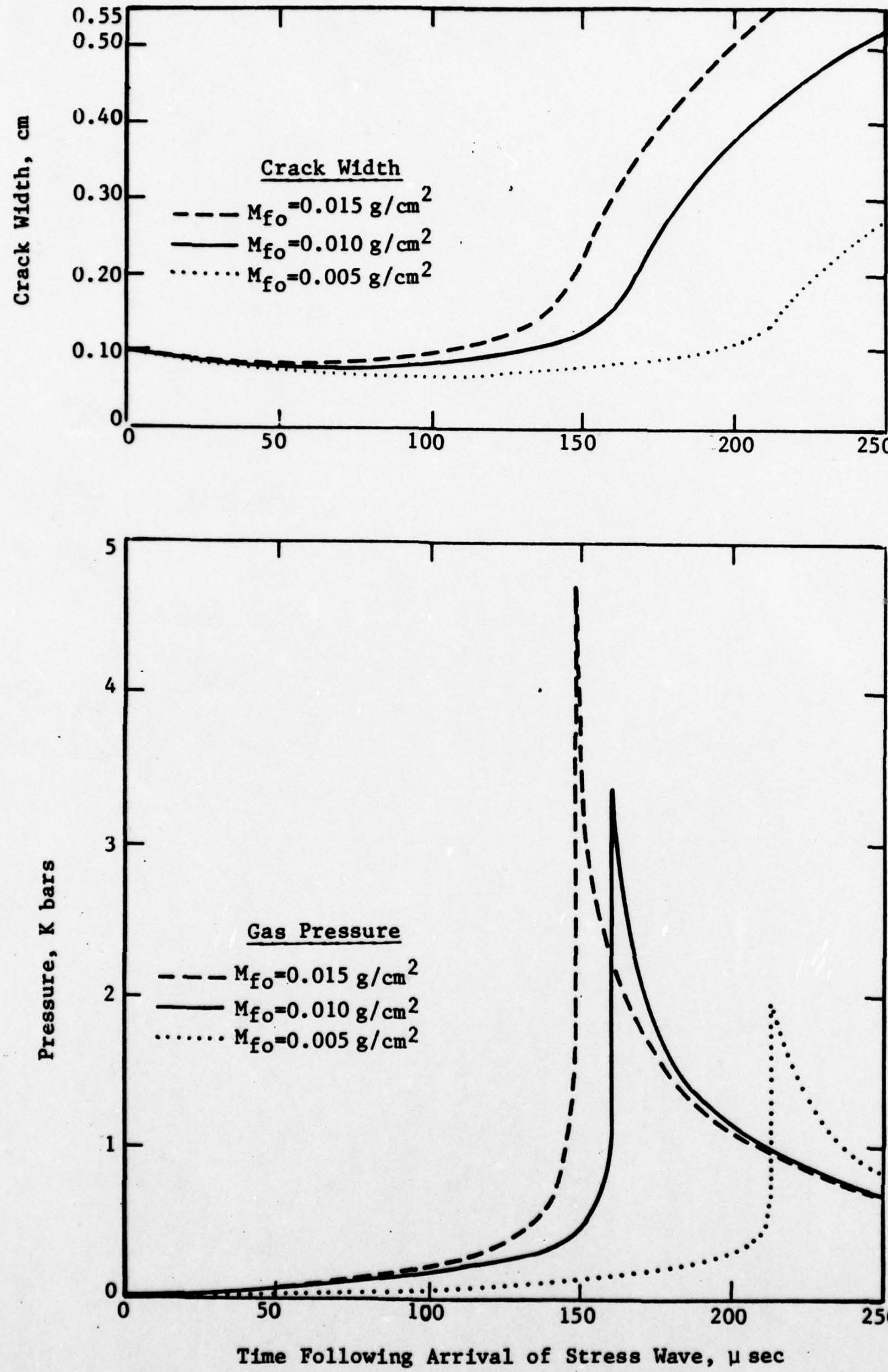

Figure 11. Consequences of Varying Initial Foam Mass (M_{fo})

TABLE 4. PARAMETRIC VALUES FOR THREE SELECTED CRACK CONDITIONS

Parameter	Case 1 Values	Case 2 Values	Case 3 Values
Q_s	100 cal/g	150 cal/g	200 cal/g
I_o*	0.30 bars sec/cm	0.45 bars sec/cm	0.60 bars sec/cm
C_{wo}	0.15 cm	0.10 cm	0.05 cm
ΔP	34 bars	68 bars	102 bars
P_o**	17 bars	34 bars	51 bars
M_{fo}	0.005 g/cm^2	0.010 g/cm^2	0.015 g/cm^2

* Impedance $I = I_o$ (1+0.0002 P(bars))

** Foam temperature and temperature distribution of solid propellant varied with P_o according to Figure 20 in the appendix

Resultant pressure transients are presented in Figure 12 for the three cases. Notice that peak pressures differ by an order of magnitude. It suggests that pressure transients will vary widely from crack to crack depending upon the propellant properties and how the crack develops, ignites and burns.

To assess the likelihood of detonation by the predicted pressure transients we shall use the threshold shock wave amplitudes (P) and durations (t) found by de Longuiville [4] to initiate a composite HMX-nylon by impact. Results are presented in Figure 13. The curve represents a constant weighted impulse P^2t. It separates test results in which detonation did and did not occur. Notice that weighted impulse represents a good criterion for constant shock wave pressures.

In that our pressure predictions are time dependent, the results of Figure 13 are not directly applicable. Nevertheless one can gain a rough measure of where we stand with respect to detonation by integrating the square of the predicted pressures over small times of the order of μseconds following the peak pressures.

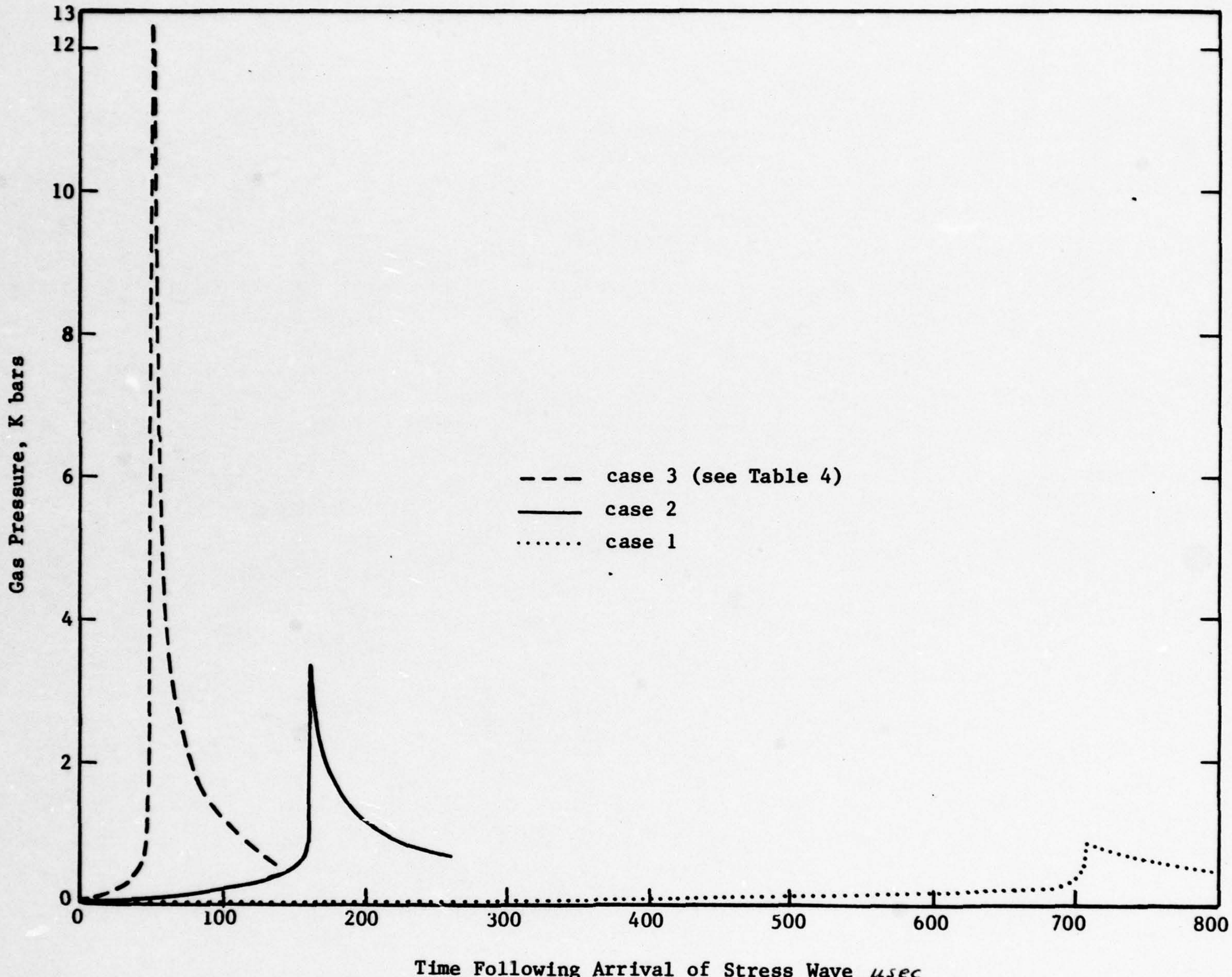

Figure 12. Pressure Transients for Three Crack Conditions

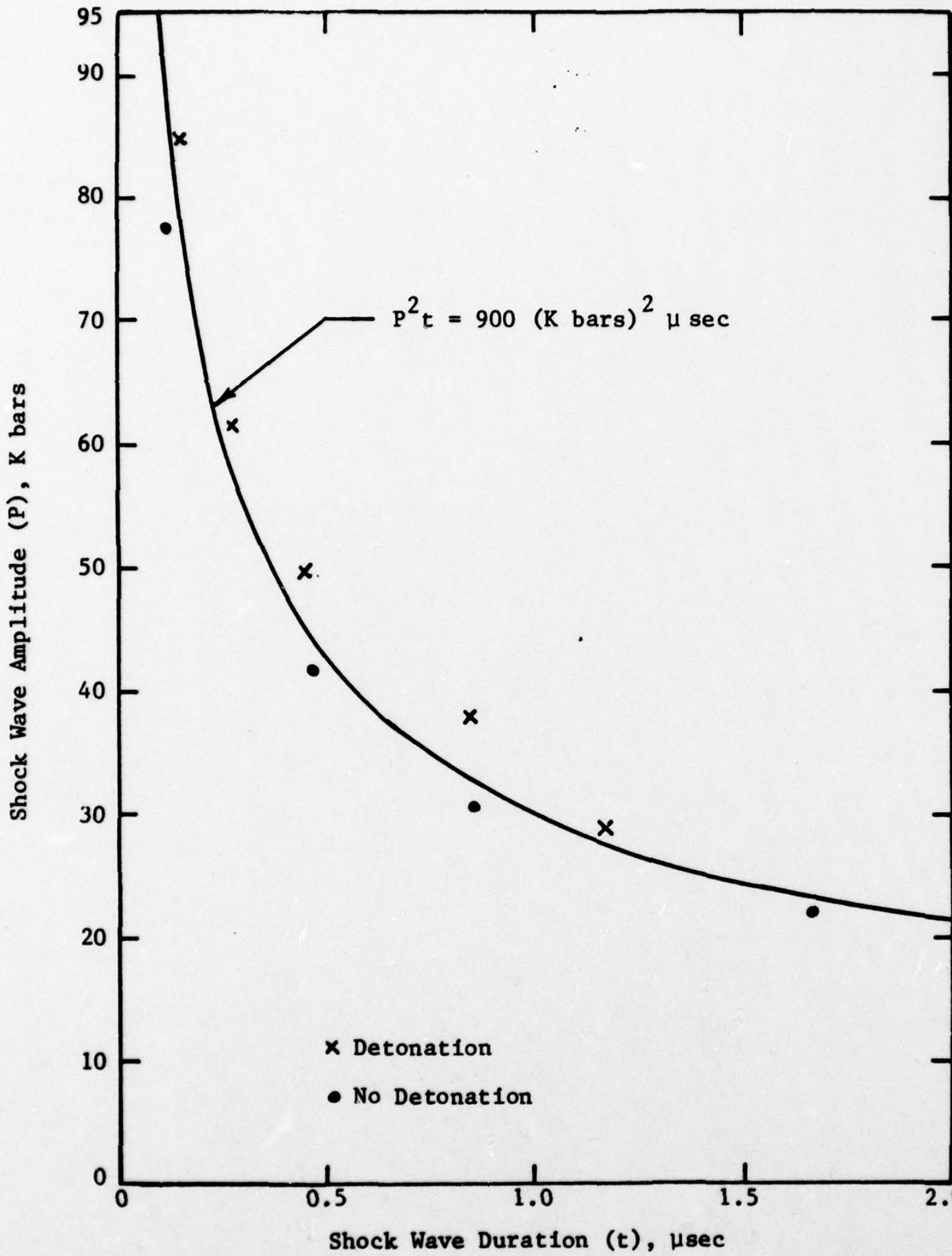

Figure 13. Impact Results from Ref. [5] for HMX-Nylon Explosive

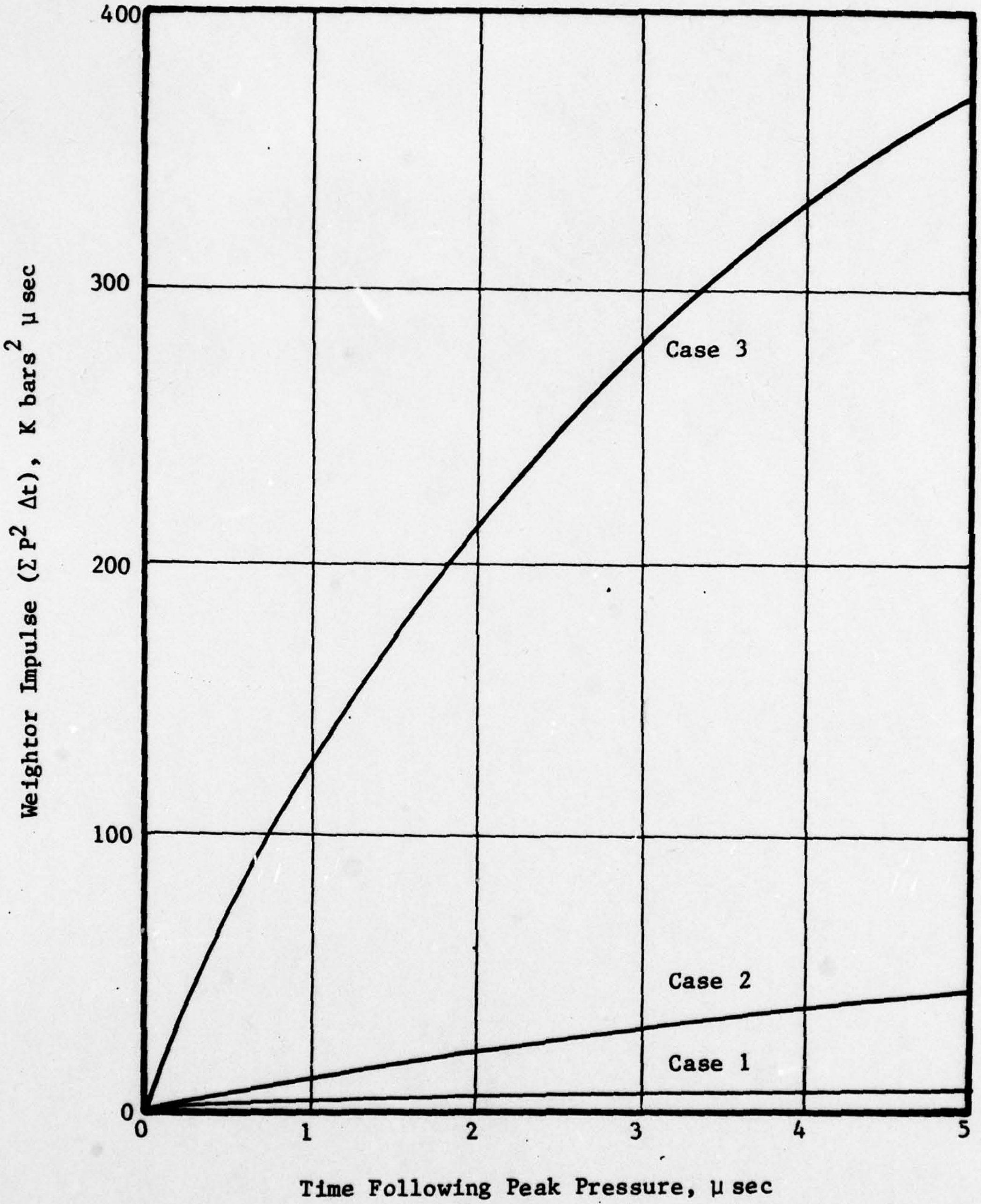

Figure 14. Integral of P^2 Over Time for Three Crack Conditions of Table 4

3.3 Multiple Cracks

From IITRI experience with burning explosive materials in closed bombs [10] it has been found that Composition B and PBX 9404 undergo multiple cracking prior to a violent explosion or high-order detonation. Two facts support the presence of multiple cracks. The first is random firing of ionization probes placed within 4 x 4 inch cylinders of the two secondary explosives. Random firing commenced when the pressure reached about 70 bars. The second is fragments of Composition B (see Figure 15) found in the bomb following sudden venting of the bomb. Explosive fragments varied in dimension from about 1/10 inch to 1 inch. All fragment surfaces were covered with a "frozen" melt layer indicating that they were burning prior to sudden pressure relief.

The presence of multiple burning cracks introduces the problem of the effect of pressure transients upon neighboring cracks of similar orientation. Of concern is the fact that the pressures produced in a crack are greater than the applied stress wave. The result is an enhanced stress wave leaving the crack that can then interact with the next burning crack. By this process more and more pronounced pressure transients and stress waves can result.

Here we shall consider three sets of identical parallel cracks. The cracks are identical to those considered earlier. They are described by case 1, case 2, and case 3 in Table 4.

Figure 16 illustrates the results for a series of identical case 1 cracks. Notice that the pressure transients become more pronounced with each succeeding crack in an accelerating fashion. Much of the pressure increase is attributable to progressive decreases of the crack width. At least seven cracks are needed to achieve pressures of the order of 10 kbars.

Figures 17 and 18 present similar results for case 2 and 3 cracks, respectively. In each of the above cracks the pressures rise more steeply to their peaks than illustrated for case 1 cracks in Figure 16. Steep pressure rises, are of course, more conducive to detonation. Also fewer cracks are needed to develop pressures of the order of tens of kbars with case 2 and 3 cracks than required with case 1 cracks.

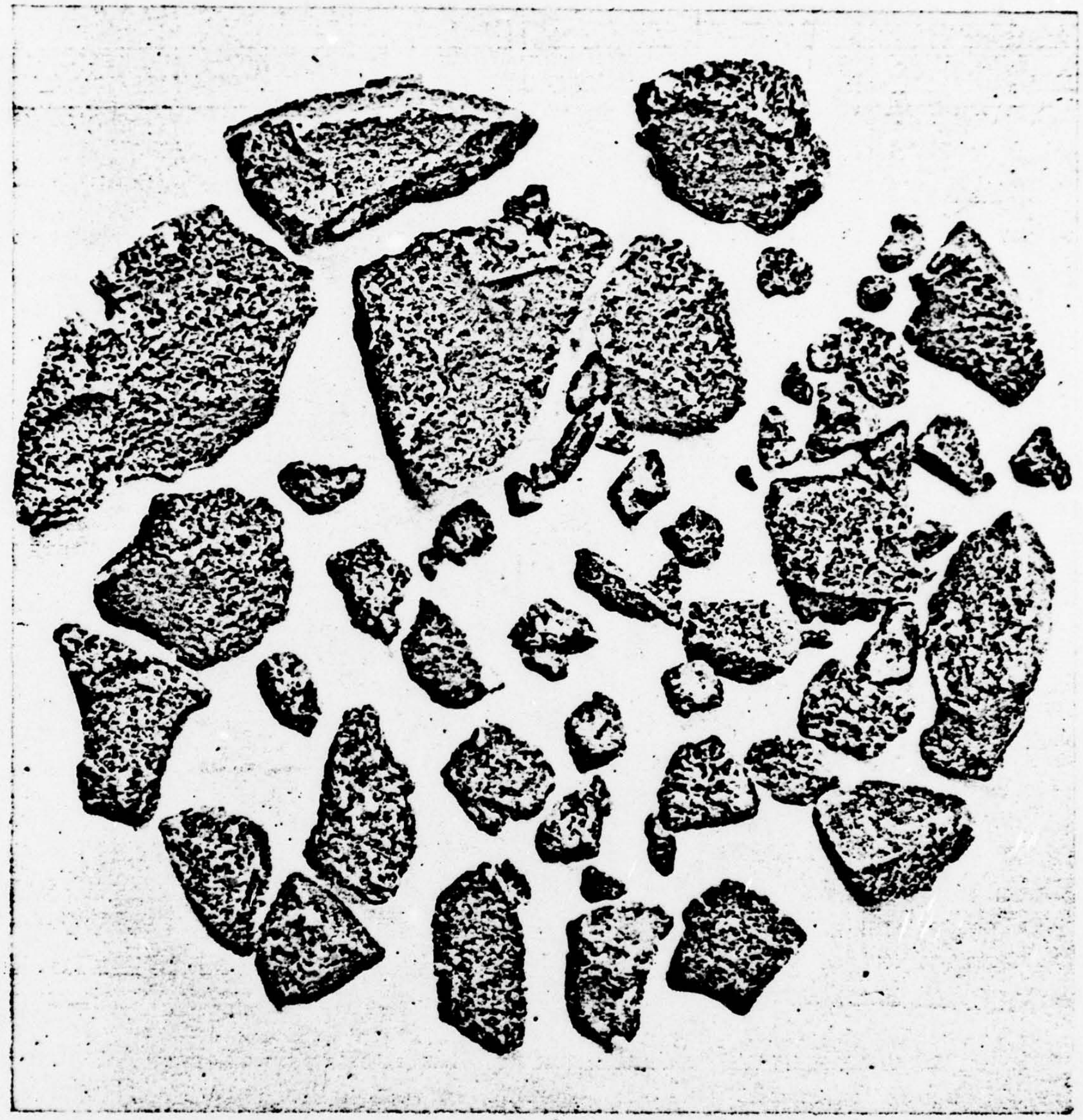

Figure 15. Composition B Fragments Found in Closed Bomb Following Sudden Pressure Relief

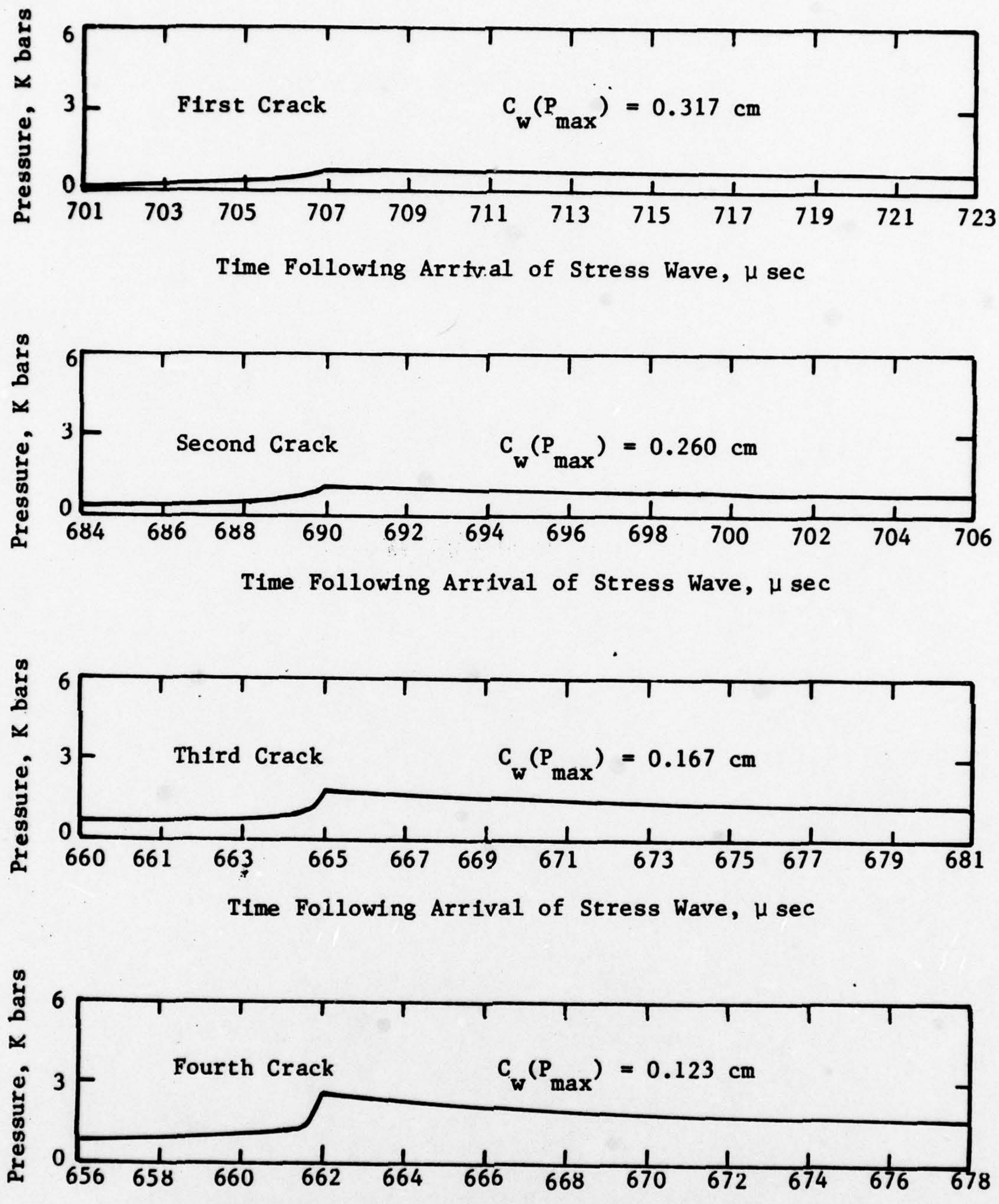

Figure 16. Multiple Cracks (case 1)

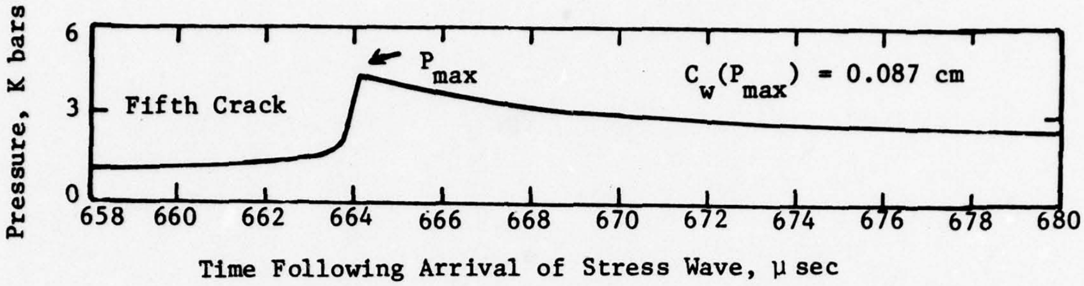

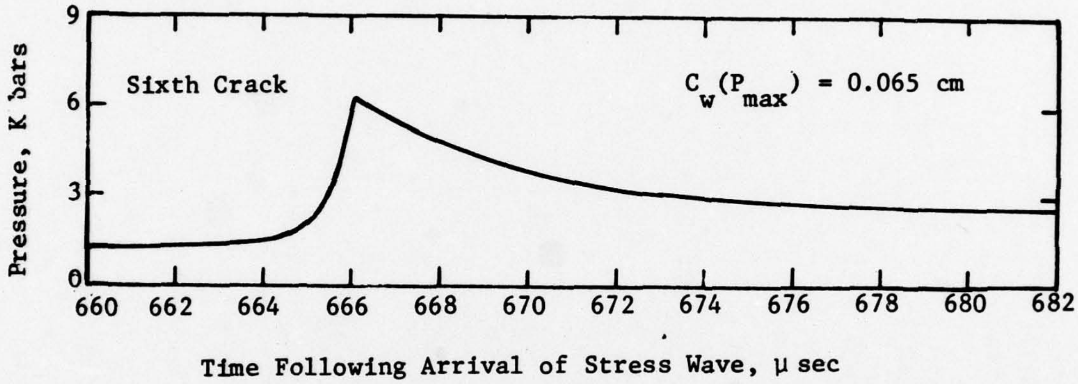

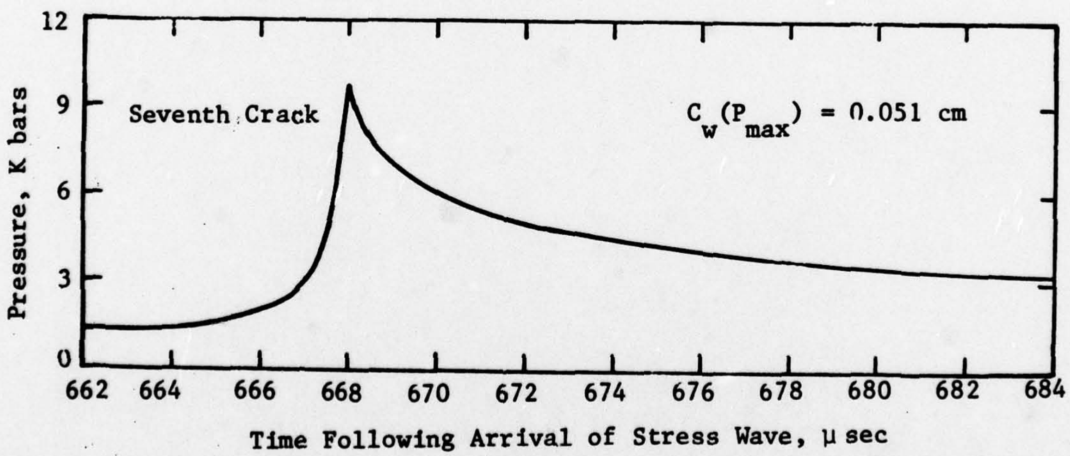

Figure 16. Multiple Cracks (case 1) (concluded)

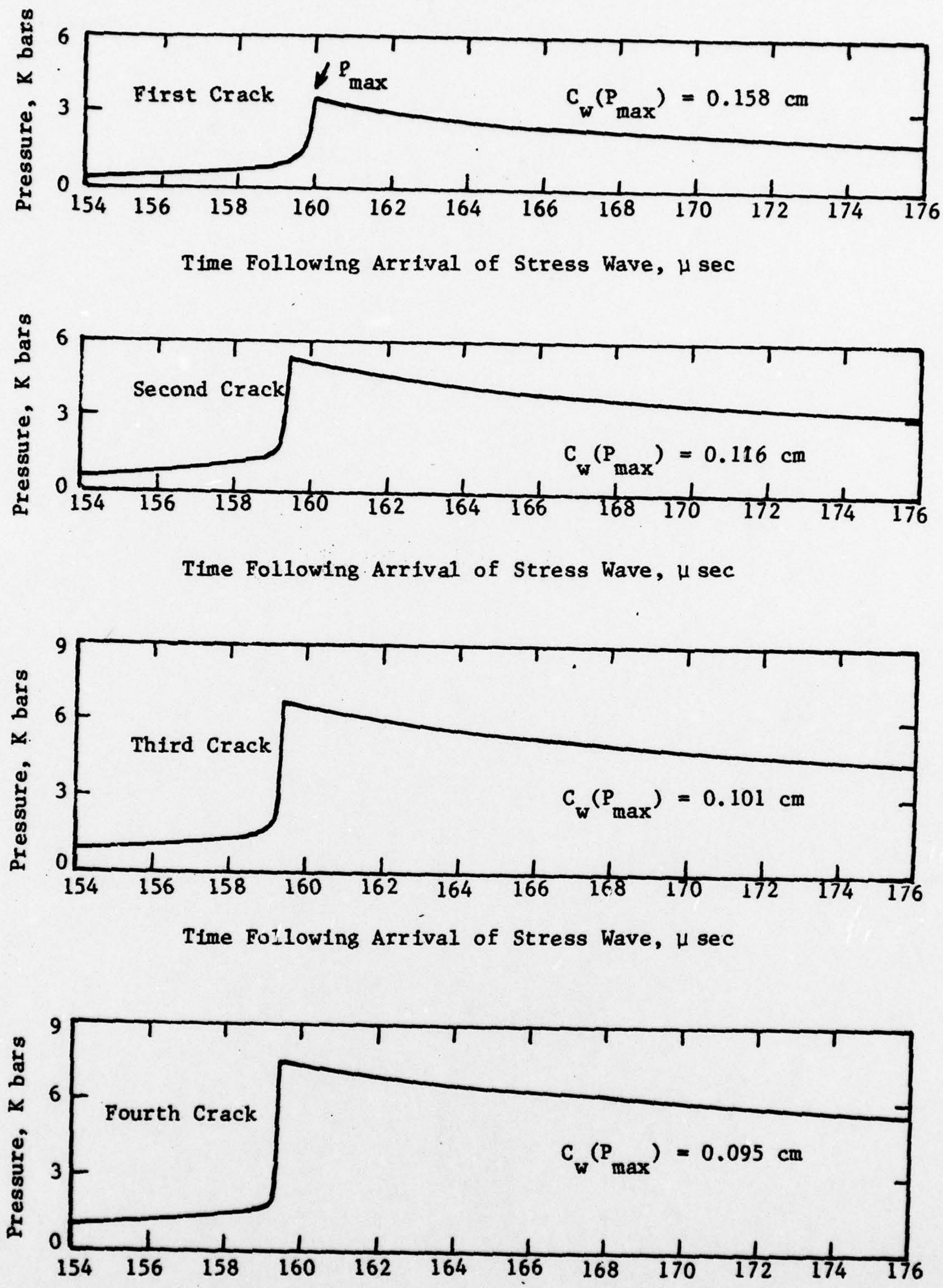

Figure 17. Multiple Cracks (case 2)

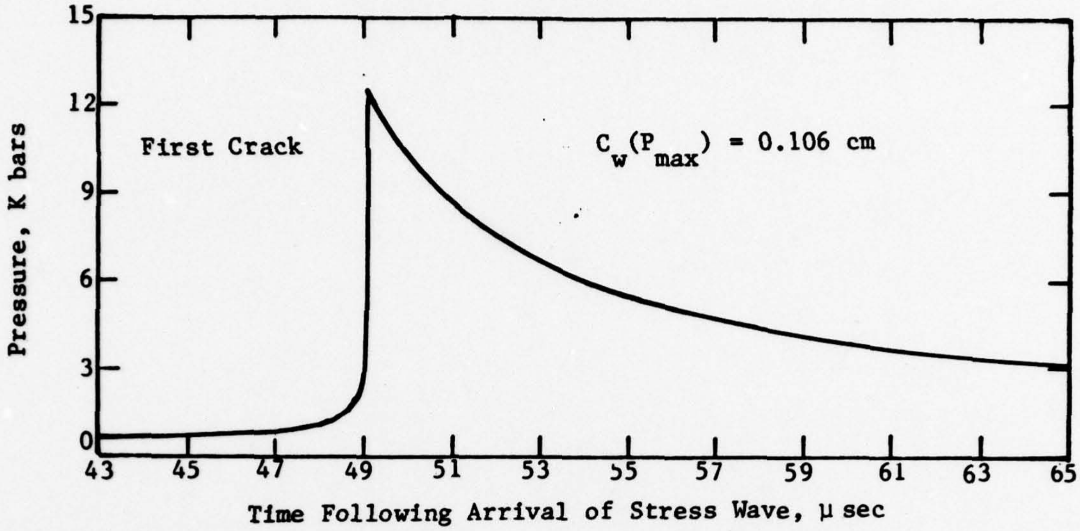

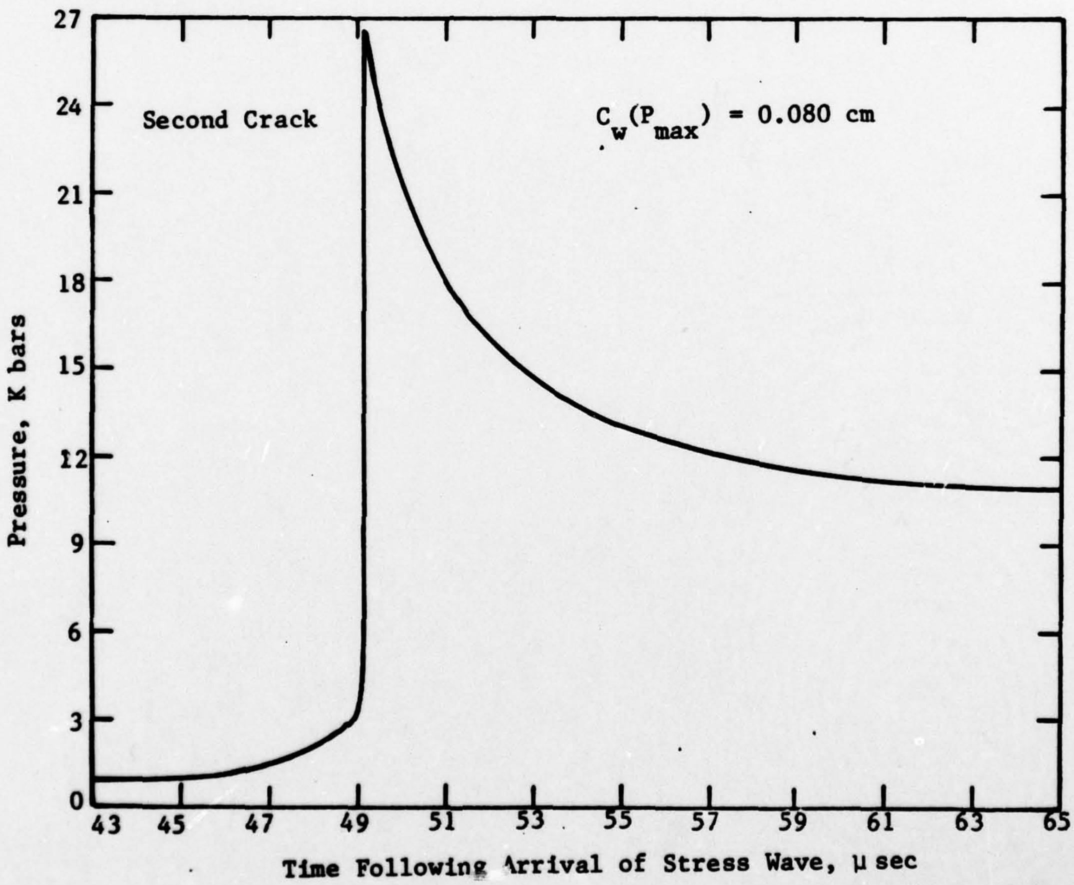

Figure 18. Multiple Cracks (case 3)

The results of Figures 16, 17, and 18 suggest that multiple cracks may lead to detonation provided enough cracks are involved in the sequential fashion indicated. This hypothesis suggests that large propellant motors are more susceptible to detonation than small motors. It is consistent with unreported IITRI observations in which a few hundred pounds of secondary high explosives (HE) burned freely, without event, while a few thousand pounds of the same HE detonated under the same burning condition. Each test result was replicated several times.

Figure 14 illustrates values of the integral of the square of the transient pressures represented in Figure 12 as a function of time. Notice that the values of the integral for cases 1 and 2 are at least an order of magnitude less than the threshold value of 900 $(\text{kbars})^2$ μsec cited in Figure 13 for constant pressures. On the other hand the integral for case 3 achieves values of similar magnitude after several μseconds.

4. SUMMARY, CONCLUSIONS AND FUTURE NEEDS

4.1 Summary/Conclusions

This study examined the consequence of various propellant properties and crack conditions upon pressure transients produced in burning cracks. Pressure transients are accentuated with propellants having large:

- internal heats Q_s
- propellant impedances I
- melt layers

Of key importance in the production of pronounced pressure transients is the presence of

- substantial foam masses and temperatures that cause rapid gas evolution early in the crack expansion phase
- large amplitude stress waves that accelerate burning by partially collapsing cracks and minimizing subsequent crack expansion

It was shown that pressure transients produced in a single crack can vary widely depending upon propellant properties and crack conditions. Pressure transients produced in cracks are always greater in magnitude than the applied stress wave. As a consequence more pronounced stress waves are applied to neighboring cracks of similar orientation which in turn produce more pronounced pressure transients. By this process pressure transients become more pronounced with each succeeding crack.

Numbers of sequential cracks needed to yield pressures/durations known to initiate HMX-nylon [4] vary with crack conditions. For the most severe crack condition considered (see Figure 18) only a few cracks are needed; for the least severe crack condition considered (see Figure 16) 10 or more cracks may be needed.

The above detonation hypothesis, of course is predicted upon the presence of multiple burning cracks. It suggests that huge rocket motors are more conducive to detonation than smaller motors.

4.2 Future Needs

4.2.1 Analyses

While the previous results suggest a likely mechanism of detonation, it remains to determine whether or not the assumed melt masses, crack widths and pressures are realistic. Such answers can be achieved by providing a foam layer in the IITRI computer code [1] used to study the dynamic effects of gas flow into cracks from a cavity of high pressure/temperature combustion gases. At present this code accounts for propellant heating by convection and burning. It predicts dynamic burning rates, crack contraction/expansion by stress waves, and gas pressures. Each of the above vary with crack location as well as with time.

Once revised the code can be used to determine transient foam masses/temperatures and crack widths following exposure of a crack to cavities containing gases at elevated pressures and temperatures. Of key concern are the conditions (propellant, crack, cavity) producing pronounced foam masses and temperatures and minimal crack widths.

4.2.2 Experiments

In addition to the above analyses, certain experimental data are needed. The first is to verify the heat-transfer coefficient used to describe heat flow from the foam to the melt interface. Two endeavors are required. The first involves measurement of the mass of the foam layer during steady burning at ambient pressure. This may be achieved by extinguishing the burning, and removing the "frozen foam" by use of acetone. The "frozen foam" would then be weighed and used in conjunction with the foam mass at 34 or 68 bars (Subsection 2.1.3) to define the heat-transfer coefficient as a function of foam temperature.

Secondly experiments are needed to test the detonation hypothesis advanced in Section 3. Of key concern are means for achieving substantial foam masses/temperatures and small void volumes such as may occur in cracks. Figure 19 illustrates an experimental setup with which to achieve such conditions.

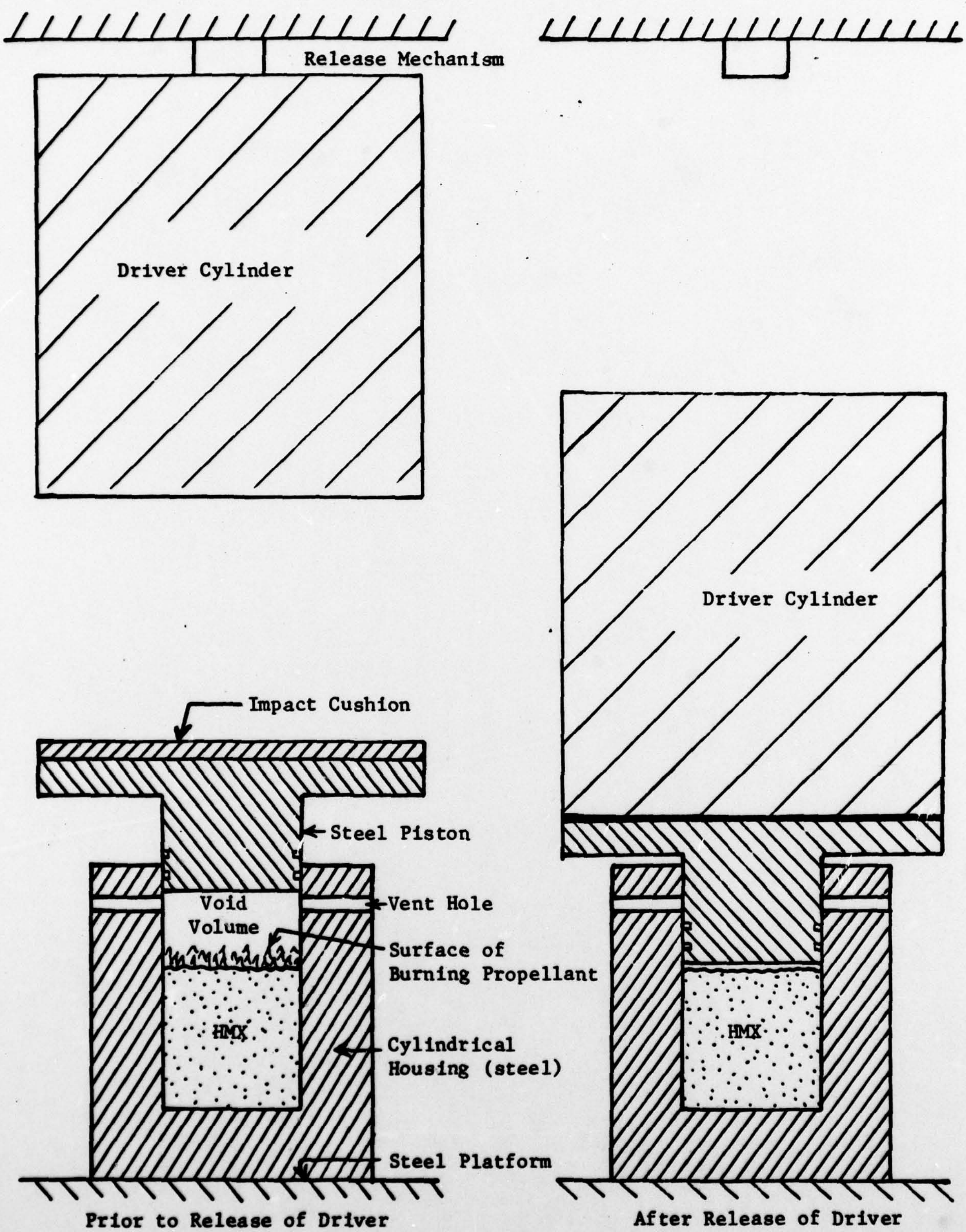

Figure 19. Setup for Simulating Crack Burning Conditions

Optimal foam masses (see Figure 3) are produced by allowing the propellant to burn at ambient pressure for several seconds until steady burning occurs. To achieve higher foam temperatures it is necessary to contract the void volume within which gases are evolved (see Figure 19). Contraction must be slow enough so that the foam can thermally respond to the increased heating brought about by the increased pressure. The above contraction does not relate to crack contraction. It merely represents means to elevate foam temperatures while decreasing the void volume. Crack simulation starts at the end of the contraction.

Preliminary calculations indicate that a contraction period of about 10 msec will be needed to achieve foam/crack conditions of comparable or greater severity as considered in this report. Foam temperatures/masses and void volume may be varied by altering:

- altitude of the driver
- height of void space
- pressure at which the propellant is allowed to burn prior to releasing the driver

In doing so foam masses will decrease only slightly during contraction of the void volume. Void volumes may be varied by at least an order of magnitude while foam temperature may be varied by at least 100°K.

Crack simulation starts with maximum contraction of the void volume. Subsequent displacements of the piston should have a negligible effect upon the void volume provided one uses a massive driver. In the simulation, the height of the void space corresponds to half that of the crack in that there is only a single burning propellant surface.

Following contraction, pressures will rise to their peaks in a matter of a few μseconds. Resultant pressure transients will vary with the foam mass/temperature and void volume. Pressures of about 10 kbars or higher are anticipated provided the foam mass approximates the value presented in Figure 3 at 1 bar of pressure and the height of the void volume is reduced to a few hundredths of a centimeter.

Several phenomena need to be considered in finalizing the design of the experimental setup shown in Figure 19. The first is heat transfer from the foam to the piston during any period of contact. In this regard the foam could be in contact with the piston for a few milleseconds and lose an appreciable fraction of its heat. Analysis suggests that the heat losses may be held to a few percent by coating the piston surface with a high-temperature paint. A layer of paint would be effective because of the short contact times. Moreover it will survive the heating.

Secondly the surface of the propellant will become concave during burning. It is caused by higher radiative fluxes at the center of the propellant surface than at its edges. Excessive deviations from the pistons surface are not desirable in that they limit the minimum void columns. In this regard deviations of the order of one-tenth of a centimeter are not of great concern because of foam displacements. Larger deviations will necessitate contouring of the piston surface to match that of the surface of the burning propellant.

Thirdly, displacements of the piston caused by elevated pressures must be insignificant as indicated earlier. For this reason the driver weight should be at least 1 kg per unit area of piston surface.

The fourth concern has to do with ignition of the propellant. Here it is desirable to achieve rapid ignition without introducing any foreign residues. One ignition possibility is to spread a layer of HMX particles over the propellant surface and ignite the particles by a flame. Ignition may be effected by directing a flame through one of the vent holes shown in Figure 19. Flames may be produced by burning a propellant within a metal tube.

The final concern has to do with gas leakage. In this regard it is expected that a close fitting piston will deter appreciable gas leakage over the short times of concern. Undercuts around the piston would create additional resistance to gas flow.

Through careful design, it should be possible to generate a wide variety of crack conditions by varying the initial burn pressure, the height of the void space, and the altitude of the driver. Initial experiments should attempt to produce detonation by simulating severe crack conditions (high foam mass/temperature, small void volume). Once detonation is achieved, followon experiments should be concerned with establishing threshold crack conditions needed to initiate the propellant.

NOMENCLATURE

a	Rate of steady burning at 1 bar of pressure (See Equation (2)), cm/sec.
C	Constant given by $2/\sqrt{KPC_p}$, $cm^2 {}^oK(sec)^{1/2}/cal$.
C_1, C_2	Constants used to describe heat-transfer coefficient h where $h=c_1(Z \exp -E/T_f)^{c_2}$.
C_g	Specific heat of gases evolved by foam at constant pressure, cal/g-^oK.
C_m	Specific heat of molten HMX, cal/g-^oK.
C_p	Specific heat of solid HMX, cal/g-^oK.
C_w	Crack width, cm.
C_{wo}	Crack width just prior to arrival of stress wave, cm.
e	Internal energy of combustion gases, cal/g.
E	Activation energy of propellant divided by gas constant, ^oK.
f	Ratio of crack area to that of planar surface, dimensionless.
h	Heat-transfer coefficient associated with heat transfer from foam to melt interface, cal/cm^2-sec-^oK.
j	Subscript used to indicate value of parameter during time step Δt_j.
I	Mechanical impedance of solid propellant, equals $I_o + 0.0002P$, bars sec/cm.
I_o	See I.
K	Thermal conductivity of solid propellant, cal/cm-sec-^oK.
M_f	Mass of unit area of foam layer, g/cm^2.
M_{fo}	Mass of foam just prior to arrival of stress wave, g/cm^2.
M_g	Mass of combustion gases, g/cm^3.

NOMENCLATURE (continued)

n	Exponent of pressure P used to describe steady burning rate $\bar{r}_f$ (see Equation (2)).
P	Pressure, bars or kbars.
ΔP	Amplitude of incident stress wave, bars.
P_o	Initial pressure of combustion gases in crack just prior to arrival of stress wave, bars.
Q_f	Sensible heat per unit mass of foam, cal/cm^2.
Q_m	Latent heat of fusion of propellant, cal/g.
Q_r	Heat of reaction of propellant, cal/g.
Q_s	Heat generated within foam per unit mass of evolved propellant, cal/g.
q	Rate of heat flow entering solid propellant, cal/cm^2-sec.
q'_j	Heat flux applied at depth x'_j during time step Δt_j, cal/cm^2-sec.
q_f	Rate of heating of unit area of foam, cal/cm^2-sec.
q_p	Rate of heat flow from foam to melt interface, cal/cm^2-sec.
$q_{i,j}$	Mean conductive heat flux at depth $\bar{X}_j$ during time step Δt_j from heat flux q_i, cal/cm^2-sec.
r	Rate of propellant melting, cm/sec.
r_f	Rate of propellant burning, cm/sec.
$\bar{r}_f$	Rate of steady burning of propellant at given pressure, cm/sec.
R	Gas constant, ^oK.
$T(x)$	Temperature of solid propellant at depth x beneath melt interface, ^oK.

NOMENCLATURE (concluded)

T_f	Foam temperature, °K.
$\bar{T}_f$	Foam temperature during steady burning at given pressure.
T_g	Temperature of combustion gases, °K.
T_m	Melt temperature of propellant, °K.
T_o	Ambient temperature of propellant, °K.
t	Time, sec.
Δt_j	j^{th} time step
W_1	Velocity of crack wall exposed to stress wave, cm/sec.
W_2	Velocity of crack wall not exposed to stress wave, cm/sec.
x_j	Depth of melt interface at end of time step Δt_j, cm.
x'_j	Depth at which flux q'_j is applied during time step Δt_j, cm.
Z	Frequency factor, one/sec.
α	Thermal diffusivity $(K/(\rho C_p))$ of solid propellant, cm^2/sec.
β	Dimensionless term (see Equation (24)) used to determine time steps.
γ	Ratio of specific heats of combustion gases, dimensionless.
ξ	Factor used to determine depths x'_j at which fluxes q'_j are applied (see Equation (23)).
ρ	Density of solid propellant, g/cm^3.
ρ_g	Density of combustion gases, g/cm^3.

APPENDIX: HMX PROPERTIES AND INITIAL TEMPERATURE DISTRIBUTIONS

Properties for HMX propellant and evolved gases are presented in Table 5.

TABLE 5 PROPERTIES OF HMX PROPELLANT AND GASES

Parameter	Value	Source
Constants a, n of Equation (2)	$a = 0.030$ cm/sec	Reference [9]
	$n = 0.86$ (dimensionless)	Reference [9]
Constants c_1, c_2 of Equation (9)	$c_1 = 7.6 \cdot 10^5$ cal/cm^2-sec-^{o}K	See Section 2
	$c_2 = 0.338$ (dimensionless)	See Section 2
C_g	0.5 cal/g-^{o}K	Assumed
C_p	0.4 cal/g-^{o}K	Reference [7]
C_m	0.5 cal/g-^{o}K	Reference [7]
f	1.5 (dimensionless)	Assumed
E	27,000^{o}K	Reference [11]
K	0.0013 cal/cm-sec-^{o}K	Assumed
Q_m	50 cal/g	Reference [7]
Q_r	1300 cal/g	Assumed
R	3517 cm/^{o}K	Assumed
T_m	555^{o}K	Reference [7]
Z	$0.5 \cdot 10^{20}$/sec	Reference [11]
ρ	1.9 g/cm^2	Reference [9]
γ	1.2	Assumed

Internal heats Q_s and propellant impedances I_o are presented in Tables 3 and 4.

Initial temperature distributions within the foam and solid propellant were varied with the initial gas pressure P_o. They are shown in Figure 20. The distributions were computed by considering constant heating of the propellant initially at a uniform initial temperature of 294^{o}K. The constant heat fluxes correspond to those associated with steady burning at the given pressure P_o. Because of heat flow prior to the start of melting, the temperatures decay more slowly with depth than steady-state temperature distributions shown in Figure 21 at the same pressure P_o.

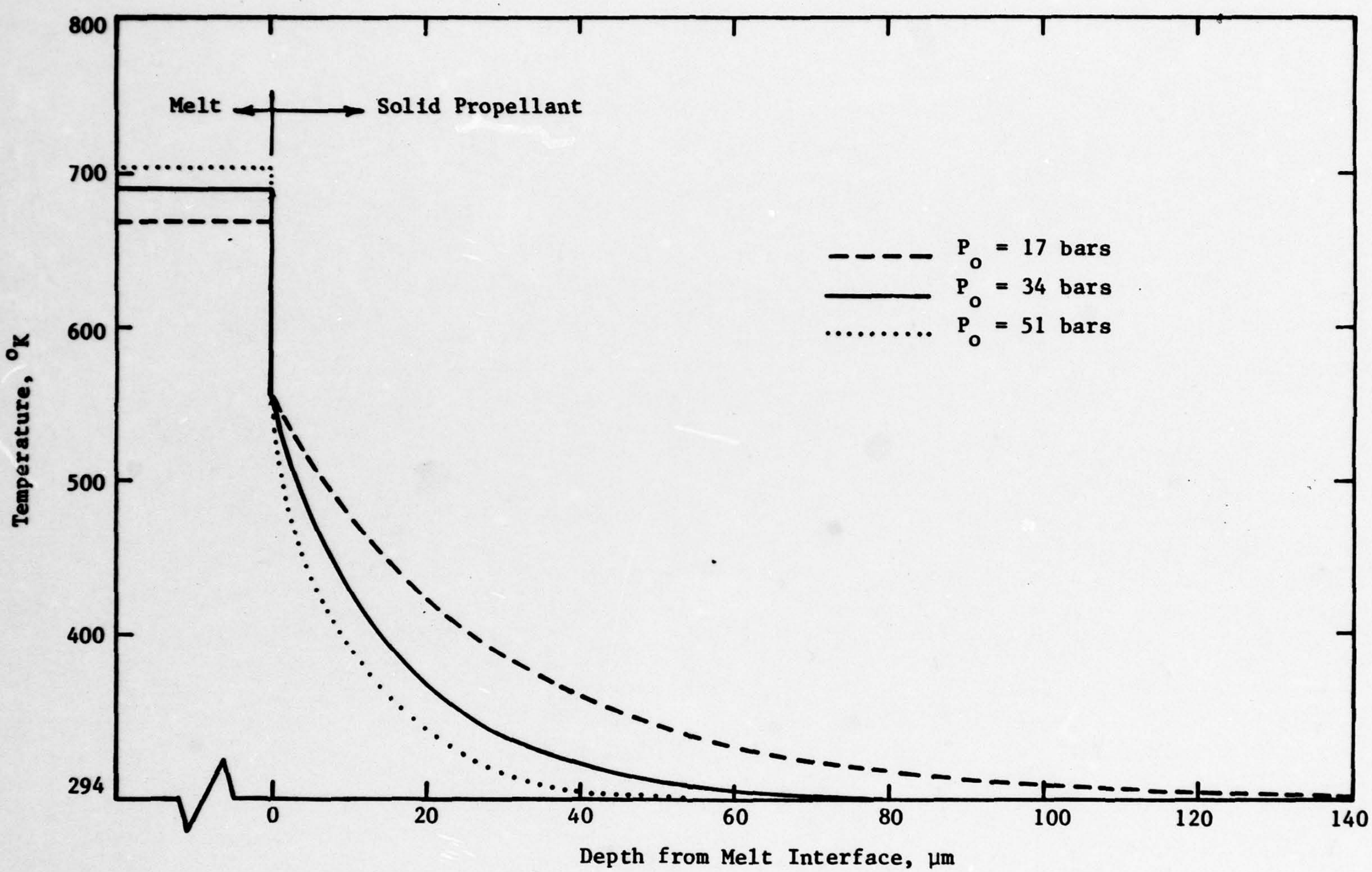

Figure 20. Assumed Temperature Profiles within HMX Immediately Prior to Arrival of Stress Wave

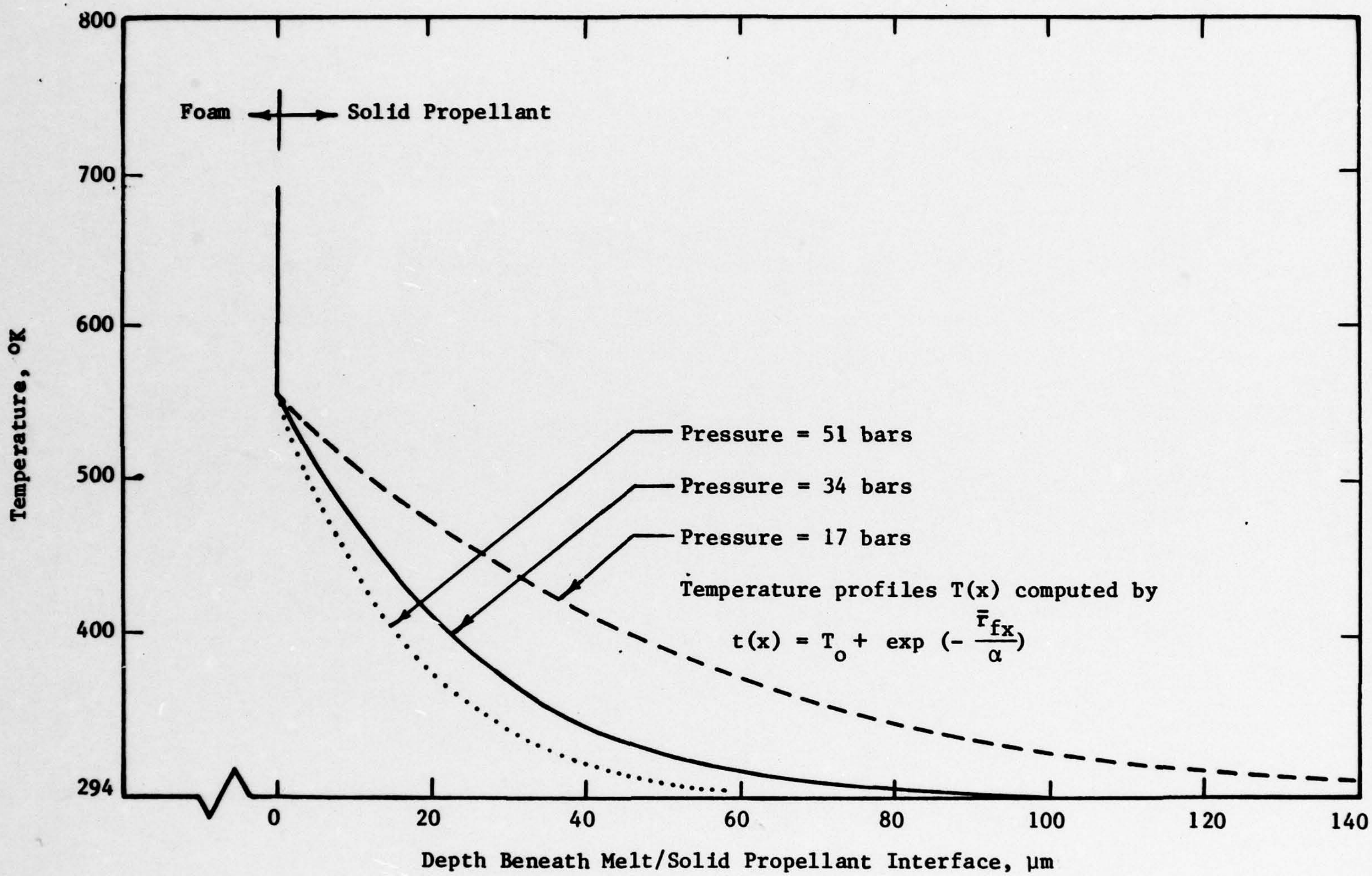

Figure 21. Predicted Temperature Profiles in Solid HMX Propellant During Steady Burning

REFERENCES

1. Takata, A. N., and A. Wiedermann, "Initiation Mechanisms of Solid Rocket Propellant Detonation", IITRI Interim Report for AFOSR, August 1976.

2. Takata, A. N., and A. Wiedermann, "Initiation Mechanisms of Solid Rocket Propellant Detonation", IITRI Second Interim Report for AFOSR, November 1977.

3. Takata, A. N., and A. Wiedermann, "Initiation Mechanisms of Solid Rocket Propellant Detonation", 14th JANNAF Combustion Meeting, Chemical Propulsion Information Agency Publication 292, December 1977.

4. de Longuiville, Y., C. Fauguignon, H. Moulard, "Initiation of Several Condensed Explosives by a Given Duration Shock Wave, Sixth Symposium (International) on Detonation, pp 16-24, August 1976.

5. Krier, H., J. S. Tien, W. A. Sirignamo, and M. Summerfeld, "Nonsteady Burning Phenomena of Solid Propellants: Theory and Experiments", AIAA J. 6 (2), February 1968.

6. Boggs, T. L., C. F. Price, D. E. Zurn, R. L. Derr, and E. J. Dibble, "The Self-Deflagration of Cyclotetramethylenetranitramine (HMX)", AIAA/SAE 13th Propulsion Conference, July 1977.

7. Takata, A. N., W. Wulff, et. al., "Study of the Behavior of Systems Containing High Explosives when Subject to Fire (U)", DASA Report 1833, July 1966.

8. Kooker, D. E., and C. W. Nelson, "Numerical Solution of Three Solid Propellant Combustion Models during Gas Pressure Transient", 12th JANNAF Combustion Meeting, CPIA Publication 273, pp 173-198, December 1975.

9. Beckstead, M. W., R. L. Derr, and C. F. Price, "The Combustion of Solid Monopropellants and Composite Propellants", 13th Symposium (International) on Combustion, pp 1047-1056, 1971.

10. Takata, A. N., "Vulnerability of Nuclear Weapon Systems to Fire-Studies of Burning Explosives", DASA Report 1417, December 1963.

11. Tomlinson, W. R. Jr., "Properties of Explosives of Military", Picatinny Arsenal, Technical Report 1740, April 1958.